Monthly Notices
of the
ROYAL ASTRONOMICAL SOCIETY

Mon. Not. R. Astron. Soc. **419,** 1913–1929 (2012) doi:10.1111/j.1365-2966.2011.19845.x

Modelling the spectra of planets, brown dwarfs and stars using VSTAR

Jeremy Bailey★ and Lucyna Kedziora-Chudczer
School of Physics, University of New South Wales, NSW 2052, Australia

Accepted 2011 September 16. Received 2011 September 15; in original form 2011 August 23

ABSTRACT

We describe a new software package capable of predicting the spectra of Solar system planets, exoplanets, brown dwarfs and cool stars. The Versatile Software for Transfer of Atmospheric Radiation (VSTAR) code combines a line-by-line approach to molecular and atomic absorption with a full multiple scattering treatment of radiative transfer. VSTAR is a modular system incorporating an ionization and chemical equilibrium model, a comprehensive treatment of spectral line absorption using a data base of more than 2.9 billion spectral lines, a scattering package and a radiative transfer module. We test the methods by comparison with other models and benchmark calculations. We present examples of the use of VSTAR to model the spectra of terrestrial and giant planet in our own Solar system, brown dwarfs and cool stars.

Key words: radiative transfer – techniques: spectroscopic – planets and satellites: atmospheres – stars: atmospheres – brown dwarfs.

1 INTRODUCTION

Until recently, the modelling of the atmospheres of stars (e.g. Gray 2005) and that of the atmospheres of the Earth and other Solar system planets (e.g. Liou 2002) have developed largely independently. Models of stars applied to high-temperature objects with effective temperatures $T_{\rm eff} > 3000$ K, with opacity dominated by the line and continuum absorption of atoms and atomic ions, whereas planetary atmosphere models applied to cool objects $T_{\rm eff} \sim 100$–300 K, where the important processes were molecular absorption and scattering from molecules and cloud particles.

This situation changed with the discovery in the mid-1990s of the first unambiguous brown dwarf, Gl 229B. (Nakajima et al. 1995; Oppenheimer et al. 1995) and the first hot Jupiter planets beginning with 51 Peg b (Mayor & Queloz 1995; Marcy et al. 1997). Many more such objects have now been discovered and reveal that planets and brown dwarfs populate an intermediate range of temperatures not explored previously. This has led to the requirement to develop new methods to model these atmospheres that cover the effective temperature range from below 1000 K to more than 2000 K.

One widely used approach has been to adapt stellar atmosphere codes to handle the lower temperatures encountered in exoplanets and brown dwarfs. Models of this type are described for example by Tsuji et al. (1996), Allard et al. (2001), Barman, Hauschildt & Allard (2001) and Burrows, Sudarsky & Hubeny (2003, 2006). An alternative approach, and the one we follow in this paper, is to take models originally used for the atmospheres of the Earth or other Solar system planets and adapt them to handle the higher temperatures needed for exoplanets and brown dwarfs. Such an approach has been described by Marley et al. (2002) and Fortney et al. (2005) who use a model based on one originally used to model the atmospheres of Titan and Uranus (McKay, Pollack & Courtin 1989; Marley & McKay 1999).

One important difference between the techniques used in stellar atmosphere modelling and in Earth atmosphere modelling is the approach to radiative transfer. In stellar atmospheres, simplified treatments of scattering, such as the assumption of isotropic scattering, are commonly adopted. This is justified by the fact that scattering is in most cases not an important source of opacity in stellar atmospheres, and where it does become significant, in the form of Rayleigh scattering from molecules in cool stars, and scattering from electrons in hot stars, the phase functions are forward–backward symmetric. Scattering from clouds and aerosols in the Earth atmosphere can, however, result in strongly forward peaked phase functions, and to properly model such cases, radiative transfer methods that more rigorously handle multiple scattering with anisotropic phase functions are needed. While these techniques build on the classic work of astronomers such as Chandrasekhar and van de Hulst, much recent development of such methods has been in the context of Earth atmosphere research (e.g. Liou 2002).

Clouds are now known to be important not just in the atmospheres of all the Solar system planets, but in many brown dwarfs and even in late M dwarfs. Thus for all these objects, a more rigorous treatment of radiative transfer is desirable. Such an approach is particularly important for modelling the reflected light from exoplanets, because the angular dependence of scattering is an important factor in determining the phase variation around a planet's orbit (e.g. Seager, Whitney & Sasselov 2000; Cahoy, Marley & Fortney 2010).

In this paper, we describe the methods used in the Versatile Sofwtware for Transfer of Atmospheric Radiation (VSTAR) atmospheric modelling software. VSTAR was originally developed as a way of modelling the spectra of the Solar system planets, and an

★E-mail: j.bailey@unsw.edu.au

early version of it is described by Bailey (2006). In this paper, we describe the current version of VSTAR which can now handle a wide range of atmospheres ranging from those of the coolest Solar system planets up to stars with temperatures of ∼3000 K, and thus including the brown dwarfs and hot Jupiter-type exoplanets.

2 THE VSTAR MODEL

2.1 Ionization and chemical equilibrium

The Ionization and Chemical Equilibrium (ICE) package of VSTAR is used to determine the equilibrium chemical composition of an atmospheric layer given its elemental abundances, pressure and temperature. ICE handles gas-phase chemistry, ionized species and the formation of solid and liquid condensates. Full details of the methods employed in this package will be described elsewhere, so only a brief description is given here. The techniques used are similar to those described by Tsuji (1973), Allard et al. (2001) and Lodders & Fegley (2002). For each compound considered in the model, the equilibrium constant of formation K_f from the elements is required. These are used in a set of equations for the mass balance of each element, and for the charge balance to solve for the abundances of each molecular species. K_f is related to the Gibbs free energy of formation $\Delta_f G^o$ through

$$\Delta_f G^o = -RT \ln K_f, \quad (1)$$

where R is the gas constant. This relationship is indicative of the link between the technique we use based on equilibrium constants, and the alternative technique for chemical models based on minimization of the total Gibbs free energy of the system (Sharp & Huebner 1990; Sharp & Burrows 2007). Both $\Delta_f G^o$ and K_f are functions of temperature (T) and are available in standard compilations of thermochemical data. Our main source of thermochemical data was the fourth edition of the National Institute of Standards and Technology (NIST)-JANAF thermochemical tables (Chase 1998). We used data from Lodders (1999, 2004) for several compounds for which the JANAF data have been shown to contain errors. Additional sources of thermochemical data were Barin (1995) and Robie & Hemingway (1995).

Some important species, however, do not have data in any of these tabulations, and for some others the available data do not extend to sufficiently high temperatures for stellar atmosphere models. For a number of gas-phase species, we have therefore calculated our own thermochemical data. To do this, we first calculate the partition function using the spectroscopic constants of the molecule. We use a rigid rotator harmonic oscillator model (with additional corrections for anharmonicity and centrifugal distortion) for the rotational and vibrational levels, and direct summation over the electronic levels (Mayer & Mayer 1940). The thermodynamic functions can then be derived from the partition function and the dissociation energy of the molecule. The techniques are essentially the same as those used in constructing the NIST-JANAF thermochemical tables (Chase 1998) for gas-phase species, and we have tested our methods by reproducing results published in these tables. Species we have calculated new thermochemical data for include FeH, CrH, CaH, TiH, RbCl and RbF.

Our thermochemical model currently includes 143 gas- and condensed-phase compounds of 27 elements. While this is not as extensive as some other models, we have been careful to include all species listed as important in previous studies such as Burrows & Sharp (1999). Our chemical model predictions show good agreement with previous results such as those of Lodders & Fegley (2002) and Sharp & Burrows (2007). Fig. 1 shows the results of calculations of the mixing ratios, or mole fractions, for a number of important species at 1 atm pressure over a range of temperatures. It can be directly compared with fig. 17 of Sharp & Burrows (2007). The model can easily be expanded by adding new species to our thermochemical data base.

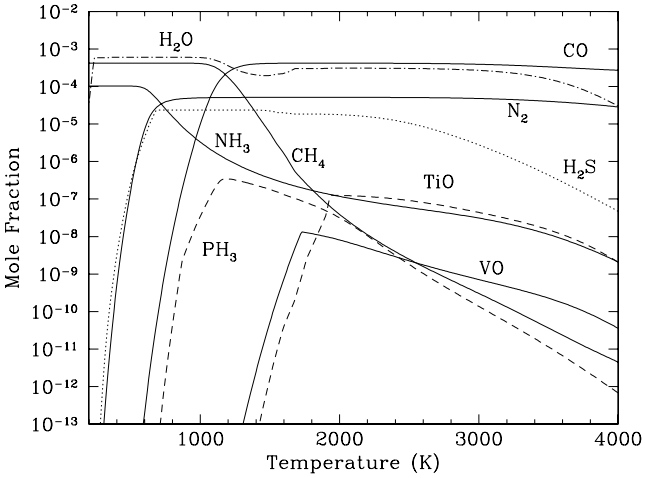

Figure 1. Mixing ratios of several important species as a function of temperature for a solar composition gas at 1 atm pressure calculated with our chemical equilibrium model. The results can be compared with fig. 17 of Sharp & Burrows (2007).

Our current model assumes true equilibrium chemistry in that when condensates form, the condensed phase is assumed to remain in equilibrium with the gas phase. This assumption is commonly made in such models. However, it may not be true in real cases since condensed material can fall under gravity and rain out of the system. Models that take account of this 'rainout' process are described by Marley et al. (2002) and Freedman, Marley & Lodders (2008).

2.2 Molecular absorption lines

Absorption lines due to rovibrational and electronic transitions of molecules are the most important features of the spectra of planets, brown dwarfs and the coolest stars. For use with VSTAR, we have collected a line data base that currently contains more than 2.9 billion lines. The line lists used with VSTAR are listed in Table 1. The line parameters are in a variety of different formats. The essential data needed for all lines are the line position (as wavelength or wavenumber), the line intensity and the lower state energy of the transition (usually given in cm^{-1} or eV).

Line intensity is usually given in one of the three forms. HIgh resolution TRANsmission (HITRAN), Gestion et Etude des Informations Spectroscopiques Atmosphériques (GEISA) (see Section 2.2.1) and similar lists give a line intensity S_0 in units of cm molecule^{-1} (sometimes given as cm^2 mol^{-1} cm^{-1}) at a reference temperature T_0. For HITRAN, T_0 is 296 K, but some other lists use a different reference temperature.

The line intensity at temperature T is then calculated using (Rothman et al. 1998)

$$S = \frac{S_0 Q(T_0)}{Q(T)} \frac{\exp(-c_2 E_l/T)}{\exp(-c_2 E_l/T_0)} \frac{[1-\exp(-c_2\nu_0/T)]}{[1-\exp(-c_2\nu_0/T_0)]}, \quad (2)$$

where ν_0 is the line frequency in cm^{-1}, E_l is the lower state energy in cm^{-1}, c_2 is the second radiation constant (=hc/k) and $Q(T)$ is the partition function (or total internal partition sum).

Table 1. Molecular line lists used with VSTAR.

Molecule	List	Number of lines	Reference
39 molecules	HITRAN 2008	2713 968	Rothman et al. (2009)
50 molecules	GEISA 2009	3807 997	Jacquinet-Husson et al. (2008)
H_2O	BT2	505 806 202	Barber et al. (2006)
H_2O	SCAN	101 455 143	Jørgensen et al. (2001)
H_2O		65 912 356	Partridge & Schwenke (1997)
H_2O	HITEMP	111 377 777	Rothman et al. (2010)
HDO	VTT	697 454 528	Voronin et al. (2010)
CO_2		7088 178	Pollack et al. (1993)
CO_2	HITEMP	11 377 777	Rothman et al. (2010)
CO_2	CDSD-296	419 610	Tashkun et al. (2003)
CO_2	CDSD-1000	3950 553	Tashkun et al. (2003)
CO_2	CDSD-Venus	11 730 277	Tashkun et al. (2003)
CO	HITEMP	115 218	Rothman et al. (2010)
CO		134 421	Goorvitch (1994)
CH_4 (cool)		339,690	See text (Section 2.2.6)
CH_4 (hot)		134 862 336	See text (Section 2.2.6)
NH_3		3249 988	Yurchenko et al. (2009)
NH_3	BYTe	1138 323 351	Yurchenko, Barber & Tennyson (2011)
TiO	SCAN	12 837 150	Jørgensen (1994)
TiO		37 744 499	Schwenke (1998)
TiO		11 369 552	Plez (1998)
VO		3171 552	Plez (private communication)
CaH		124 615	Weck, Stancil & Kirby (2003a)
MgH		23 315	Weck et al. (2003b); Skory et al. (2003)
MgH		119 167	Kurucz (2005)
FeH ($F-X$)		116 300	Dulick et al. (2003)
FeH ($E-A$)		6357	Hargreaves et al. (2010)
CrH		14 255	Burrows et al. (2002)
TiH		199 073	Burrows et al. (2005)
CH	SCAN	114 567	Jørgensen et al. (1996)
CN	SCAN	2245 378	Jørgensen & Larsson (1990)
C_2		360 887	Querci, Querci & Kunde (1971); Querci, Querci & Tsuji (1974)
HCN/HNC		34 433 190	Harris et al. (2006)

Line intensities may also be quoted in the form of Einstein A coefficients (A_{21}). The line intensity S (in cm mol^{-1}) at a temperature T can be calculated from A_{21} using (Šimečková et al. 2006)

$$S = \frac{gA_{21}}{8\pi c\nu_0^2 Q(T)} \exp(-c_2 E_l/T)[1 - \exp(-c_2\nu_0/T)]. \quad (3)$$

Here g is the statistical weight of the upper level of the transition. In most cases, g can be written as $(2J + 1)g_s$, where J is the rotational quantum number of the upper state and g_s is the nuclear spin degeneracy. Different formulae are needed if hyperfine structure is included in the line list (see Šimečková et al. 2006). The g_s used in equation (3) needs to be consistent with that used in calculating the partition function (see Section 2.5.2).

In astronomical line lists, such as those of Kurucz (2005), the oscillator strength f, usually tabulated as gf or $\log(gf)$ (where g is the statistical weight) is the usual form for listing line strengths. The line intensity at temperature T can be calculated from gf using

$$S = \frac{\pi g f e^2}{m_e c^2 Q(T)} \exp(-c_2 E_l/T)[1 - \exp(-c_2\nu_0/T)], \quad (4)$$

where e is the electron charge, m_e is the electron mass and other symbols are as above.

2.2.1 *HITRAN and GEISA*

HITRAN and GEISA are compilations of molecular spectroscopic parameters designed primarily for the Earth atmosphere, but often useful for the atmospheres of other planets. Both are updated every few years with the most recent releases being HITRAN 2008 (Rothman et al. 2009) and GEISA 2009 (Jacquinet-Husson et al. 2008). The line parameters are generally best suited to low-temperature models and more complete line lists are usually needed for higher temperature atmospheres such as those encountered in brown dwarfs, hot Jupiter-type planets and stars. For example, Bailey (2009) showed that HITRAN and GEISA were significantly incomplete for water vapour line parameters at temperatures of 500–700 K encountered in the Venus lower atmosphere.

2.2.2 *HITEMP*

The HITEMP data base is a companion to HITRAN containing line data suitable for use at higher temperatures. The latest edition of HITEMP was released in 2010 (Rothman et al. 2010) and replaces an earlier edition described by Rothman et al. (1995). HITEMP contains data for five species, H_2O, CO_2, CO, NO and OH. The data format is the same as that used in HITRAN, and HITEMP is consistent with HITRAN, in the sense that lines common to both data bases have the same line parameter values, although HITEMP includes many lines not in HITRAN.

2.2.3 *Water vapour – H_2O*

Water vapour is an important absorber in atmospheres ranging from stars to the terrestrial planets. A number of line lists are available

for water vapour at high temperatures. These include the HITEMP list (Rothman et al. 2010), the SCAN list (Jørgensen et al. 2001), the list of Partridge & Schwenke (1997) and the BT2 list (Barber et al. 2006). Comparisons of the various lists have been reported by Allard, Hauschildt & Schwenke (2000), Jones et al. (2003) and Bailey (2009). We normally use the BT2 list which is the most extensive and is based on the accurate dipole moment surface of Schwenke & Partridge (2000). The HITEMP list for H_2O is based on BT2.

BT2 includes only the main isotopologue of water ($H_2{}^{16}O$). The VTT list of Voronin et al. (2010) provides a similar list for HDO. In the atmosphere of Venus, deuterium is enhanced over terrestrial abundances by a factor of 100–150, so HDO absorption is significant. Line data for a range of other isotopologues of water at 296 and 1000 K are available from the Spectra Information System (http://spectra.iao.ru) at the Institute of Atmospheric Optics, Tomsk. These data are based on the analysis of Schwenke & Partridge (2000).

2.2.4 *Carbon dioxide – CO_2*

Carbon dioxide is an important constituent of terrestrial planet atmospheres. Until recently, it has not been thought to be important in giant planet atmospheres. However, recent results from transiting extrasolar planets (Swain et al. 2009a,b) suggest CO_2 may be important in these atmospheres as well. Recently, CO_2 has also been detected in brown dwarfs (Yamamura, Tsuji & Tanabe 2010). At low temperatures, HITRAN, GEISA or CDSD-296 (Carbon Dioxide Spectroscopic Databank; Tashkun et al. 2003) can be used. High-temperature line lists include the list described by Pollack et al. (1993) and the CDSD-1000 list (Tashkun et al. 2003). The latter list contains more than 3 million lines and is complete to an intensity of 10^{-27} cm mol^{-1} at 1000 K.

The dense CO_2 atmosphere of Venus provides a particular challenge to the modelling of CO_2 absorption with pressures up to 90 bar of almost pure CO_2 and requires a line list with a much deeper intensity cut-off than is normally necessary. The list of Pollack et al. (1993) is the one that has normally been used for modelling the Venus deep atmosphere. However, an alternative is the CDSD-Venus list, a version of the CDSD list with a deeper cut-off of 10^{-30} cm mol^{-1} at 750 K.

The HITEMP (Rothman et al. 2010) list for CO_2 is based on the CDSD line lists.

2.2.5 *Carbon monoxide – CO*

Carbon monoxide is significant in terrestrial planet atmospheres and is also observed in Titan. It also becomes important in high-temperature atmospheres where equilibrium chemistry favours CO over CH_4. For high temperatures, the HITEMP line list (Rothman et al. 2010) or the list of Goorvitch (1994) can be used.

2.2.6 *Methane – CH_4*

Methane is an important absorber in the atmospheres of the Solar system giant planets and in Titan. It has been detected in the atmospheres of extrasolar giant planets (Swain, Vasisht & Tinnetti 2008). It is also important in brown dwarfs, the presence of methane absorption features in the near-infrared (near-IR) being the defining characteristic of the T dwarf class.

However, methane has a complex spectrum due to the presence of coincidences between its four vibrational modes that result in a series of interacting states known as polyads, spaced at intervals of about 1500 cm^{-1}. Most line data are either based on experimental measurements or on effective Hamiltonian models, which exist only for the lowest few polyads. The Spherical Top Data System (STDS) software of Wenger & Champion (1998) can be used to generate line lists from these effective Hamiltonian models. A good model has recently been obtained (Albert et al. 2009) for the ground state and the lowest three polyads (the dyad, pentad and octad), and this allows reliable prediction of the low-temperature methane spectrum from 0 to 4800 cm^{-1}. This model is used in the 2008 update of the methane line parameters in HITRAN (Rothman et al. 2009). A preliminary model is available for the next polyad, the tetradecad (Robert et al. 2001; Boudon, Rey & Loete 2006).

Above 4800 cm^{-1}, many of the line parameters included in HITRAN are empirical measurements at room temperature originating from Brown (2005). These mostly lack lower state energies (HITRAN lists fictitious lower state energies of 555.5555 or 333.3333) and so cannot be used to derive reliable line intensities at other temperatures. However, some lines in the 5500–6150 cm^{-1} region have empirical lower state energies derived from measurements at multiple temperatures from Margolis (1990) and Gao, Kassi & Campargue (2009).

Recently, much improved data for the low-temperature methane spectrum over the range 1.26–1.71 μm (5852–7919 cm^{-1}) have become available from laboratory measurements described by Wang, Kassi & Campargue (2010), Wang et al. (2011), Campargue et al. (2010) and Mondelain et al. (2011). These data are based on a combination of room temperature and cryogenic (∼80 K) measurements that allow empirical determinations of lower state energies, and includes deep cavity ring down spectroscopy of the weak lines in the window regions between the strong absorption band systems. An application of this list to the spectrum of Titan is reported by de Bergh et al.. (2011).

For low-temperature atmospheres, such as the Solar system giant planets or Titan, we use a composite list that combines the laboratory data described above, as well as data described by Nikitin et al. (2010, 2011), with HITRAN data from 0 to 4800 cm^{-1}. We use STDS to fill in the remaining gap in coverage between 4800 and 5500 cm^{-1}. An early version of this list and its application to Titan is described by Bailey, Ahlsved & Meadows (2011). The current version of the list is further improved by including the most recent data of Wang et al. (2011) and Mondelain et al. (2011).

For high-temperature atmospheres, such as those of brown dwarfs and hot Jupiters, we use a line list computed with the STDS software (Wenger & Champion 1998) up to $J = 60$ for most band systems, and up to $J = 50$ for the most complex system modelled (the tetradecad–pentad). This gives a list of nearly 135 million lines. Because the effective Hamiltonian model of Albert et al. (2009) involves high-order polynomial fits to empirical data usually limited to the range up to J = 20–30, it is not suitable for extrapolation to these high J values. We instead use the low-order effective Hamiltonian parameters of Borysov et al. (2002). These provide a poorer fit to observed line positions (∼0.5 cm^{-1}) but allow more reliable extrapolation to high J. For most purposes, we use a smaller list extracted from the full list with a line intensity cut-off of 10^{-27} cm mol^{-1} at 1500 K, giving a list of 15.8 million lines.

While this approach to the hot methane spectrum is similar to that used by other groups modelling brown dwarf and exoplanet spectra (e.g. Borysov et al. 2002; Homeier, Hauschildt & Allard 2003; Freedman, Marley & Lodders 2008), it is important to understand

that while these models include high rotational levels, they do not include higher vibrational levels that are needed at these temperatures and many hot band systems are therefore missing. Methane band strengths will therefore be underestimated by amounts that will increase for shorter wavelengths and higher temperatures.

Above 6500 cm^{-1}, there is little useful methane line data for high temperatures. The low-temperature line list can be used but will omit both hot bands and high J transitions. An alternative is available in the form of low-resolution absorption coefficients, band models or k-distribution parameters for methane (Strong et al. 1993; Irwin et al. 2006; Karkoschka & Tomasko 2010). The first two sets cover the near-IR, and the latter extends through the visible as well. However, these data are not in an ideal form for use with line-by-line programs such as VSTAR and are not designed for high-temperature use. The optimal way to use such data sets is in conjunction with the correlated-k method (Goody et al. 1989).

2.2.7 *Ammonia – NH_3*

Ammonia is present in the atmospheres of Jupiter and Saturn, and is also found in cool brown dwarfs where it is seen most easily through a feature at 10.5 μm (Cushing et al. 2006). The spectrum of ammonia, has until recently, presented similar problems to methane. The line parameters in HITRAN only include lines up to 5295 cm^{-1} and have not been updated since the 2000 edition. However, recently a new line list (the BYTe list) for hot NH_3 (up to ∼1500 K) has been published by Yurchenko et al. (2011). It contains more than 1.1 billion lines covering the range 0–12 000 cm^{-1}. An NH_3 list for use up to 300 K and covering 0–8000 cm^{-1} was described by Yurchenko et al. (2009).

2.2.8 *Metal oxides – TiO and VO*

Bands of titanium oxide (TiO) and vanadium oxide (VO) are distinctive features of the spectrum of M-type stars. There are several line list available for TiO from Jørgensen (1994), Schwenke (1998) and Plez (1998). The lists cover five isotopologues of the TiO molecule. Comparisons of the lists can be found in Allard et al. (2000) and Pavlenko et al. (2006). The VSTAR data base also includes a VO line list provided by Plez (private communication), which is part of the line lists assembled by Gustafsson et al. (2008).

2.2.9 *Metal hydrides – CaH, MgH, FeH, CrH and TiH*

Bands due to electronic transitions of metal hydrides are seen in M-type stars and some cooler objects. A line list for MgH is described by Weck et al. (2003b) and Skory et al. (2003). This list, and a similarly formatted list for CaH (Weck et al. 2003a) can be found on the website of the University of Georgia Molecular Opacity Project.[1] An alternative MgH list which includes two additional MgH isotopologues is available from Kurucz (2005).

Line lists are also available for FeH (Dulick et al. 2003), CrH (Burrows et al. 2002) and TiH (Burrows et al. 2005). These line lists are all similarly formatted. They cover only the most abundant isotopologue of each molecule, though methods for determining line positions for other isotopologues are described. The Dulick et al. (2003) line list for FeH covers the $F - X$ band, but absorptions in the $E - A$ band are also important in the 1.6-μm region. These

[1] http://www.physast.uga.edu/ugamop/index.html

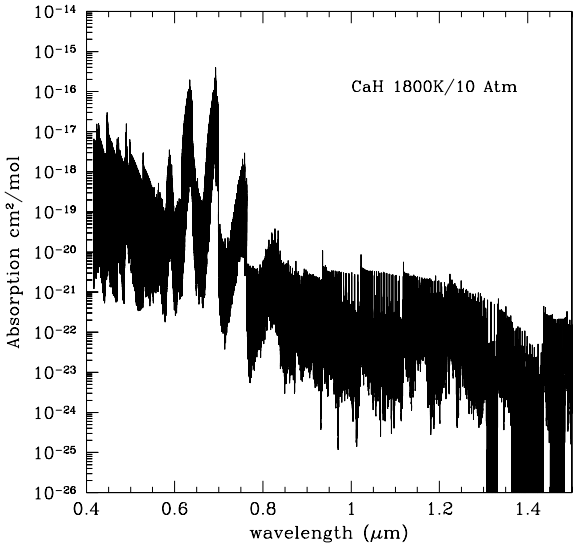

Figure 2. Monochromatic absorption (in cm^2 $molecule^{-1}$) of CaH at a temperature of 1800 K and a pressure of 10 atm.

are available from a recent empirically based line list described by Hargreaves et al. (2010).

2.2.10 *CH, CN and C_2, HCN/HNC*

These bands are present in cool stars and become particularly strong in carbon stars. Line lists available from Jørgensen et al. (1996) (CH), Jørgensen & Larsson (1990) (CN), Querci et al. (1971) and Querci et al. (1974) (C_2) and Harris et al. (2006) (HCN/HNC) are included in the VSTAR data base.

2.2.11 *Absorption plots*

Sharp & Burrows (2007) have presented plots of the monochromatic absorption (in cm^2 $molecule^{-1}$) for many molecular species present in brown dwarf or giant exoplanet atmospheres. We have made similar plots for the molecular species described above. In all but one case, our plots look essentially the same as those given by Sharp & Burrows (2007). The exception is CaH where our absorption plot, given in Fig. 2, shows the well-known absorption bands at 0.638 and 0.683 μm in M dwarfs, which are absent in fig. 9 of Sharp & Burrows (2007) for the same temperature and pressure.

2.3 Atomic lines

While molecular lines are most important in the coolest objects, lines of the alkali metals are significant in brown dwarfs and exoplanets, and many other atomic lines become important in M stars. VSTAR can make use of atomic line data in the format of the Kurucz line lists, or that of the Vienna Atomic Line Database (VALD; Piskunov et al. 1995; Kupka et al. 1999).

2.4 Line profiles

The default treatment of spectral line profiles in VSTAR is to use a Voigt line shape in the line core, approximated using the methods described by Humlicek (1982) and Schreier (1992), out to 20 Doppler widths from the line centre. In the line wings, a van

Vleck–Weisskopf profile is used which has a line shape function $\phi(\nu)$ of the form (van Vleck & Weisskopf 1945)

$$\phi(\nu) = \frac{1}{\pi}\left(\frac{\nu}{\nu_0}\right)\left[\frac{\gamma}{(\nu-\nu_0)^2+\gamma^2} + \frac{\gamma}{(\nu+\nu_0)^2+\gamma^2}\right], \quad (5)$$

where ν is frequency, ν_0 is the line centre frequency and γ is the line half-width. In most cases, this is essentially identical to a Lorentzian, but this profile provides the asymmetry that is needed at microwave wavelengths or with very broad lines, and goes to zero at zero frequency.

In general, it is found that continuing this profile out to large distances from the line centre overestimates the absorption in the far wings. In cases where the precise far wing behaviour is important, VSTAR allows the line wings to be modified by multiplying by a correction factor, usually called a χ factor. For example, the far line wings of CO_2 are known to be sub-Lorentzian (Perrin & Hartmann 1989; Tonkov et al. 1996), and the correct profile is important in modelling the spectra of the 'windows' in the Venus night-side spectrum (e.g. Meadows & Crisp 1996).

Where the precise line wing shape is not critical, it is usually sufficient to cut off the line profiles at a distance from the line centre, which can be chosen according to the typical line strengths and widths but usually ranges from 20 to 100 cm^{-1}. This approach improves the speed of computation. In either this case, or the χ factor case, the line intensities are adjusted to ensure that the integrated line strength is not changed from its original value.

The line profile requires a value for the pressure-broadened line half-width (γ in equation 5). HITRAN, GEISA and similarly formatted files such as HITEMP and CDSD include linewidth data in the form of an air-broadened line half-width coefficient γ_0 (in $cm^{-1}\,atm^{-1}$, quoted for the reference temperature T_0), a self-broadened line half-width and a temperature exponent n for the linewidth, such that

$$\gamma(T) = \gamma_0\left(\frac{T_0}{T}\right)^n. \quad (6)$$

Linewidths for different transitions of a molecule vary, and are usually found to depend primarily on the rotational quantum numbers of the levels involved in the transition. Variation with the vibrational quantum numbers is much smaller, and is often ignored in empirical models for the line shape.

Linewidths depend on the type of gas responsible for the broadening. Hence the air-broadened widths given in HITRAN-type files are not usually what is needed, as we generally want the linewidths for broadening in H_2 and He (for giant planet and brown dwarf atmospheres) or CO_2 (for terrestrial planets). Unfortunately, the data available on these alternate broadening gases are rather incomplete.

Table 2 shows the relative linewidths due to broadening in different broadening gases, averaged over many transitions. The linewidths are relative to that due to broadening in N_2. Some general trends can be identified in the table. For example, helium always produces the smallest broadening. O_2 broadening is always less than that due to N_2. CO_2 produces the largest broadening. However, H_2 is sometimes less than, and sometimes more than, N_2. These trends can be used as a rough guide, when no broadening information is available for a specific broadening gas.

Broadening for a mixture of gases can be obtained by averaging the broadening coefficients weighted by their partial pressures (or volume mixing ratios). Table 2 gives values for air (taken as 80 per cent N_2 and 20 per cent O_2) and an H_2/He mixture typical of a giant planet or brown dwarf atmosphere (85 per cent H_2 and 15 per cent He) obtained from the other values in the table.

VSTAR includes specific models for the linewidths of several of the more important gases. For H_2O broadened in CO_2, we use the model described by Bailey (2009) based on the data of Delaye, Hartmann & Taine (1989). For H_2O broadened in H_2 and He, we use the data from Gamache et al. (1996). For NH_3 broadened by H_2, He, N_2 and O_2, we use the results of Brown & Peterson (1994) for the dependence of width on the J and K quantum numbers, and the temperature exponents are from Nouri et al. (2004). For CO, we use the model for the J dependence from HITRAN (Rothman et al. 2005) for air and from Régalia-Jarlot et al. (2005) for H_2. When CH_4 line data are taken from HITRAN, the air-broadened width from HITRAN is used for H_2/He broadening also, since Table 2 shows little difference in the two cases. For other sources of CH_4 line data, the broadening is based on data from Pine (1992).

Atomic line lists usually give width data in the form of three coefficients for natural (γ_n), van der Waals (γ_w) and Stark (γ_s) broadening. Stark broadening is usually negligible at the temperatures considered here. The linewidth γ needed for equation (5) can be calculated from

$$\gamma = \frac{1}{4\pi c}\left[\gamma_w(N_H + c_1 N_{H_2} + c_2 N_{He})\left(\frac{T}{10\,000}\right)^{0.3} + \gamma_n\right], \quad (7)$$

where N_H, N_{H_2} and N_{He} are the number densities of atomic hydrogen, molecular hydrogen and helium. c_1 and c_2 are coefficients for the relative broadening effects of H_2 and He as compared with H, which can be derived from the polarizabilities of the different species. If γ_w and γ_n are not available, they are calculated using methods described by Kurucz & Avrett (1981).

2.5 Partition functions

The calculation of line intensities from data tabulated in the line lists using equations (2), (3) or (4) requires the partition function $Q(T)$ of the molecule or atom defined by

$$Q(T) = \sum g_i \exp\left(\frac{-E_i}{kT}\right), \quad (8)$$

where E_i is the energy of level i relative to the ground state, g_i is its statistical weight and the sum is to be taken over all rotational, vibrational and electronic levels.

Table 2. Relative broadening effects of different broadening gases.

Lines	Broadened by							References
	H_2	He	N_2	O_2	CO_2	Air	H_2/He	
NH_3	0.832	0.370	1.0	0.693		0.939	0.818	Brown & Peterson (1994)
CH_4	1.017	0.643	1.0	0.943		0.989	0.961	Pine & Gabard (2003)
CO	0.85	0.64	1.0	0.90	1.30	0.98	0.82	Burch, Singleton & Williams (1962); Hartmann et al. (1988)
H_2O	0.777	0.221	1.0	0.661	1.50	0.932	0.694	Gamache, Lynch & Brown (1996)
CO_2	1.41	0.59	1.0	0.81	1.20	0.962	1.287	Burch et al. (1969)

2.5.1 Molecular partition functions

VSTAR uses molecular partition functions from a range of sources. Polynomial approximations for the partition functions of many molecules for temperatures from 1000 up to 9000 K or higher are given by Sauval & Tatum (1984) and Irwin (1981). A subroutine for calculating the partition functions of all molecules and isotopologues in HITRAN is provided with that data base and is described by Fischer et al. (2003). The HITRAN partition functions are valid over the temperature range from 70 to 3000 K. An updated version of the HITRAN partition functions has recently been published by Laraia et al. (2011), but the work described in this paper used the earlier versions from Fischer et al. (2003). Partition functions can be reconstructed from data in the NIST-JANAF thermochemical tables (Chase 1998). These tables do not list the partition functions explicitly, but the thermochemical properties listed for gas-phase substances are derived from partition functions. The partition function can be calculated from the tabulated data using methods described by Irwin (1988).

Partition functions can also be calculated directly from spectroscopic constants using methods already described in Section 2.1. In some cases, it is possible to calculate molecular partition functions by direct summation over energy levels as in the partition functions for H_2O from Vidler & Tennyson (2000) and CH_4 from Wenger, Champion & Boudon (2008).

2.5.2 Partition functions and nuclear spin

In comparing the molecular partition functions from different sources, it was noted that the partition functions from HITRAN (Fischer et al. 2003) had values which were larger than those from most other sources by integer factors. This is due to the use in HITRAN of a different convention for the treatment of nuclear spin states. The convention in astrophysics is not to count nuclear spin states as distinct states in equation (8). As stated by Irwin (1981), 'the statistical weights are divided by ... the product of the nuclear spin statistical weights'. It is clear from the descriptions of the HITRAN partition functions in Fischer et al. (2003), Šimečková et al. (2006) and Laraia et al. (2011) that a different convention is adopted in HITRAN, and some other spectroscopy literature, where the corresponding statistical weights include nuclear spin states.

The consequence is that on the HITRAN convention, partition functions $Q_{\rm HIT}$ are numerically larger than astrophysical partition functions $Q_{\rm ast}$ by a factor defined as follows:

$$Q_{\rm HIT}(T) = Q_{\rm ast}(T) \prod_{j=1}^{n} (2I_j + 1), \tag{9}$$

where I_j are the nuclear spins of the n atoms contained in a molecule. With $I = 0$ for carbon and oxygen, 1/2 for hydrogen and 1 for nitrogen, these factors become 4 for H_2O, 16 for CH_4 and 24 for NH_3.

In many cases (e.g. equation 2), partition functions are divided such that these integer factors will cancel out. However, this is not the case when line intensities are calculated from Einsten A coefficients using equation (3). In this case, it is important that the statistical weights ($g_{\rm s}$) and partition function use the same convention. For example, for H_2O lines, if an astrophysical partition function is used, the statistical weights for the ortho- and para-states of water are 3/4 and 1/4, but if the HITRAN partition function is used they are 3 and 1.

Table 3. Continuum absorption processes in VSTAR.

Process	Reference
H^- free–free	Bell & Berrington (1987)
H^- bound-free	Wishart (1979)
H bound-free and free–free	Gray (2005)
H_2^- free–free	Bell (1980)
H_2–H_2 CIA	Borysow (2002)
	Borysow et al. (2001)
H_2–He CIA	Borysow et al. (1989, 1997)
	Borysow & Frommhold (1989)
O_2–O_2 and O_2–N_2 CIA	Smith & Newnham (1999, 2000)
H_2–N_2 CIA	McKellar (1989)

2.5.3 Atomic partition functions

Partition functions for atoms and atomic ions in VSTAR are calculated using a modified version of the PFSAHA subroutine taken from the ATLAS9 software of Kurucz.[2]

2.6 Continuum processes

A number of continuum absorption processes are included in VSTAR as described in Table 3.

2.6.1 Bound–free and free–free continuum absorption

Bound-free and free–free absorptions of a number of species are important in stellar atmospheres, and some of these processes remain significant at the cooler temperatures of hot Jupiters and brown dwarfs. The processes included in VSTAR are listed in Table 3. These processes are sufficient for the range of temperatures and wavelengths currently studied using VSTAR. A wider range of continuum processes would need to be incorporated to extend the applicability of VSTAR to higher temperatures and into ultraviolet (UV) wavelengths (see e.g. Sharp & Burrows 2007; Gustafsson et al. 2008).

2.6.2 Collision-induced absorptions

Collision-induced absorption (CIA) due to H_2–H_2 pairs is important in the Solar system giant planets where it shows up a distinct strong spectral feature at 2.1 μm (see Fig. 5 for the spectrum of Jupiter in this region). This absorption is also important in brown dwarf, hot Jupiters and M dwarfs. We incorporate this absorption by interpolating in tables provide by Borysow.[3] Three different tables are needed to cover the full temperature range using calculations by Borysow (2002) (60–350 and 400–1000 K) and Borysow, Jørgensen & Fu (2001) (1000–7000 K). H_2–He CIA is also included using data from Borysow, Jørgensen & Zheng (1997), Borysow, Frommhold & Massimo (1989) and Borysow & Frommhold (1989).

Other CIAs included in VSTAR are absorption in the O_2 near-IR bands (Smith & Newnham 1999, 2000) which is needed for the Earth atmosphere and H_2–N_2 CIA which occurs in the Titan atmosphere and for which data are available from McKellar (1989).

[2] http://kurucz.harvard.edu/programs/atlas9
[3] http://www.astro.ku.dk/ aborysow/programs

2.7 Scattering

Scattering processes are often treated in stellar atmosphere codes as just an additional source of opacity which can be added to that due to gas absorption. However, VSTAR uses a more rigorous treatment that requires a full description of scattering. In addition to the optical depth contribution, we need to know the single scattering albedo, ϖ, and the phase function, $P(\theta)$, that describes the angular distribution of scattered light.

Single scattering albedo is defined as

$$\varpi = \frac{\sigma_\mathrm{s}}{\sigma_\mathrm{s} + \sigma_\mathrm{a}} = \frac{\sigma_\mathrm{s}}{\sigma_\mathrm{e}}, \tag{10}$$

where σ_e, σ_a and σ_s are the extinction, absorption and scattering cross-sections per particle.

2.7.1 Rayleigh scattering from molecules

VSTAR includes models for the Rayleigh scattering due to air, H, H_2, He, N_2 and CO_2 or any mixture of these gases. The wavelength dependence of the scattering cross-section of H_2 is from Dalgarno & Williams (1962). Those of H and He are from Dalgarno as cited by Kurucz (1970).

For the other gases, the scattering cross-section (σ) is derived from the refractive index of the gas using (Hansen & Travis 1974)

$$\sigma = \frac{8\pi^3(n(\lambda)^2 - 1)^2}{3\lambda^4 N^2} F_\mathrm{K}, \tag{11}$$

where $n(\lambda)$ is the wavelength-dependent refractive index, λ is wavelength and N is the number density (molecules cm^{-3}) of the gas measured at the same temperature and pressure as the refractive index. F_K is known as the King factor and is given by

$$F_\mathrm{K} = \frac{6 + 3\delta}{6 - 7\delta}, \tag{12}$$

where δ is the depolarization factor. For air, we use the refractive index wavelength dependence from Peck & Reeder (1972) and the King factor from Young (1981). For CO_2, the refractive index is from Old, Gentili & Peck (1971) and the King factor is from Sneep & Ubachs (2005). For N_2, the refractive index is from Cox (2000).

Rayleigh scattering is pure scattering, so it has a single scattering albedo of one, and the phase function is

$$P(\theta) = \frac{3}{4}(1 + \cos^2\theta). \tag{13}$$

2.7.2 Scattering from particles

Scattering from liquid or solid particles suspended in the atmosphere (variously called clouds, aerosols or condensates) occurs in all planetary atmospheres in the Solar system, and in brown dwarfs and M stars.

Particle scattering can be modelled using Lorenz–Mie theory, which provides a solution to Maxwell's equations that describe scattering of light from a homogenous sphere with a complex refractive index $n + ik$, and a size parameter $x = 2\pi r/\lambda$, where r is the radius of the sphere and λ is the wavelength. VSTAR uses a Lorenz–Mie scattering code from Mishchenko, Travis & Lacis (2002) that models scattering from a size distribution of spherical particles. The particle size distribution can be described by a number of functional forms including power law, lognormal and gamma distributions. VSTAR can handle up to 20 particle modes, each with its own wavelength-dependent refractive index, particle size distribution and vertical distribution in the atmosphere.

The scattering code generates the extinction and scattering cross-sections per particle (σ_e and σ_s) which give the single scattering albedo according to equation (10).

It also provides the phase function $P(\theta)$ both as an array of values for different scattering angles and as an expansion in Legendre polynomials:

$$P(\theta) = \sum_{s=0}^{s_\mathrm{max}} \alpha^s P_s(\cos\theta), \tag{14}$$

which is the form required for the discrete-ordinate radiative transfer code described in Section 2.8.

If the particles are genuinely spherical (e.g. liquid droplets), then the phase function derived from the Lorenz–Mie code is appropriate. Sometimes, however, spherical models are used simply as a generic representation of solid particles which probably have a range of irregular shapes. In this case, the full spherical particle phase function is probably not a good representation. It will include angular structure in the form of features such as rainbows and glories that are specific to the particles' sphericity, and disappear for non-spherical particles (Bailey 2007). In this case, a better representation may be the Henyey–Greenstein phase function (Henyey & Greenstein 1941):

$$P_\mathrm{HG}(\theta) = \frac{1 - g^2}{4\pi(1 + g^2 - 2g\cos\theta)^{3/2}}, \tag{15}$$

where g is the asymmetry parameter defined by

$$g \equiv \langle\cos\theta\rangle = \int_0^\pi \cos\theta\, P(\theta) 2\pi \sin\theta\, \mathrm{d}\theta. \tag{16}$$

Here g is between -1 and 1, and is positive for forward scattering and negative for backward scattering. The asymmetry parameter is also provided by the Lorenz–Mie scattering code.

As well as using Lorenz–Mie theory, VSTAR can make use of pre-calculated scattering parameters derived using other methods. Scattering from non-spherical particles can be modelled using T-matrix methods (Waterman 1971; Mishchenko 1991). Codes available from Mishchenko et al. (2002) can be used to calculate the scattering properties of particles with spheroidal or cylindrical shapes or shapes described by Chebyshev polynomials in either random or specific orientations. However, T-matrix techniques are generally limited to small size parameters and can be very slow to compute. Some examples of applications of these techniques can be found in Bailey (2007) and Bailey et al. (2008a).

The aerosols that make up Titan's stratospheric haze have optical properties that can be modelled by fractal aggregates composed of many spherical particles. Models described by Tomasko et al. (2008) give the scattering properties of the Titan aerosols including optical depth, single scattering albedo and phase function in a form suitable for use with VSTAR.

2.8 Radiative transfer

The data on absorption and scattering derived by the methods described in Sections 2.2–2.7 are finally combined to provide the inputs needed for solving the radiative transfer equation. VSTAR is structured in a modular way so that a number of different approaches to radiative transfer can potentially be used. However, for most of our work, we have used the DISORT package (Stamnes et al. 1988). DISORT is a robust computer implementation of the discrete ordinate method for radiative transfer originally developed by Chandrasekhar (1960).

DISORT models the radiative transfer in a multiple layer medium, including the processes of absorption, multiple scattering and thermal emission, and allows a reflecting surface at the lower boundary and a direct beam source (e.g. the Sun) illuminating the top of the atmosphere.

The radiative transfer equation solved by DISORT has the form

$$\mu \frac{\mathrm{d}I_\nu(\tau, \mu, \phi)}{\mathrm{d}\tau} = I_\nu(\tau, \mu, \phi) - S_\nu(\tau, \mu, \phi), \tag{17}$$

where I_ν is the monochromatic radiance (sometimes referred to as intensity or specific intensity) at frequency ν, and is a function of optical depth τ, and direction μ, ϕ, where μ is the cosine of the zenith angle, and ϕ is the azimuthal angle. The source function S_ν is given by

$$\begin{aligned} S_\nu(\tau, \mu, \phi) = {} & \frac{\varpi(\tau)}{4\pi} \int_0^{2\pi} \int_{-1}^{1} P(\mu, \phi; \mu', \phi') I_\nu(\tau, \mu', \phi') \mathrm{d}\mu' \mathrm{d}\phi' \\ & + (1 - \varpi) B_\nu(T) \\ & + \frac{\varpi F_\nu}{4\pi} P(\mu, \phi; \mu_0, \phi_0) \exp(-\tau/\mu_0), \end{aligned} \tag{18}$$

where the first term describes scattering of radiation into the beam from other directions according to single scattering albedo ϖ and phase function $P(\mu, \phi; \mu', \phi')$, the second term is thermal emission, with $B_\nu(T)$ being the Plank function, and the third term is direct illumination of the atmosphere by an external source with flux $\mu_0 F_\nu$ and direction μ_0, ϕ_0 (e.g. the Sun).

The inputs required by DISORT are the vertical optical depth ($\Delta\tau$), single scattering albedo (ϖ) and phase function moments (α^s, the coefficients of the Legendre polynomial expansion of the phase function as defined in equation 14) for each atmospheric layer. The temperature at each level is also needed for thermal emission calculations.

The values of these are obtained by summing the contributions of all relevant processes for each layer of the atmosphere at each wavelength. The combined absorption due to all molecular and atomic line processes as well as related continuum processes (Sections 2.2–2.6) is called $\Delta\tau_{\mathrm{gas}}$. Rayleigh scattering (Section 2.7.1) contributes an optical depth $\Delta\tau_{\mathrm{ray}}$ which is pure scattering optical depth. Each of the p modes ($p = 1$ to $p_{\max}$) of scattering particles (Section 2.7.2) provides both a scattering optical depth $\Delta\tau^p_{\mathrm{scatt}}$ and an absorption optical depth $\Delta\tau^p_{\mathrm{abs}}$.

The total optical depth for a layer is

$$\Delta\tau = \Delta\tau_{\mathrm{gas}} + \Delta\tau_{\mathrm{ray}} + \sum_{p=1}^{p_{\max}} (\Delta\tau^p_{\mathrm{scatt}} + \Delta\tau^p_{\mathrm{abs}}). \tag{19}$$

The combined single scattering albedo for a layer is the scattering optical depth divided by the total optical depth and so is given by

$$\varpi = \frac{\Delta\tau_{\mathrm{ray}} + \sum_{p=1}^{p_{\max}} \Delta\tau^p_{\mathrm{scatt}}}{\Delta\tau}, \tag{20}$$

and the combined phase function moments (α^s for $s = 0$ to $s_{\max}$) are the phase function moments for the individual scattering components, the Rayleigh scattering (α^s_{ray}) and the p particle modes (α^{sp}), weighted according to their contribution to the scattering optical depth:

$$\alpha^s = \frac{\alpha^s_{\mathrm{ray}} \Delta\tau_{\mathrm{ray}} + \sum_{p=1}^{p_{\max}} \alpha^{sp} \Delta\tau^p_{\mathrm{scatt}}}{\Delta\tau_{\mathrm{ray}} + \sum_{p=1}^{p_{\max}} \Delta\tau^p_{\mathrm{scatt}}}. \tag{21}$$

DISORT approximates the angular distribution of the radiation field by replacing the integral term in the source function with a sum over a number of discrete zenith angles (or streams) according to the Gaussian quadrature rule. The number of streams determines how accurately the angular distribution of radiance is calculated. For many purposes where the variation with angle is reasonably smooth, we have found eight streams (four upwards and four downwards) to be adequate. However, the number of streams can be increased as necessary to provide more accurate representation of angular structure at the cost of increased computation time.

DISORT provides a number of outputs. In astronomical cases, we are mostly interested in the upward radiance and its angular dependence at the top of the atmosphere. The radiance can be determined for any emission angle and for any azimuth relative to the illuminating source. It is also possible to determine the radiation field at the surface of the planet or at intermediate levels in the atmosphere.

The radiative transfer equation only holds for monochromatic radiance. Thus to obtain the spectrum of a planet, the radiative transfer calculation must be repeated for each wavelength, and the wavelength steps made sufficiently small to resolve the spectral lines. We normally use a set of points that are equally spaced in wavenumber, and with a spacing chosen to be just sufficient to resolve the narrowest absorption lines encountered in any layer of the model. Typically, this requires several hundred thousand spectral points to be calculated.

2.9 VSTAR operation

We can now outline the full procedure for using VSTAR to calculate the spectrum of a planet, brown dwarf or star. The first steps in the process are different depending on whether we are modelling a Solar system planet (including the Earth) or an exoplanet, brown dwarf or star.

2.9.1 First step – Solar system case

In the Solar system planet case, we start with a measured profile for the temperature and pressure as a function of height. This is available for all planets in the Solar system, either from radio occultation observations or from entry probes or other *in situ* data. For Earth, there are a number of 'standard atmosphere' profiles available, and several of these are built-in to VSTAR. Some other planets have standard atmospheres, e.g. the Venus International Reference Atmosphere (VIRA; Seiff et al. 1985)

The mixing ratios of the various gases and their distribution with altitude are also generally reasonably well known from *in situ* measurement or past spectroscopic analysis. Thus for any such planet, we can start with an atmospheric profile which consists of a number of layers (typically 30–60) with the pressure, temperature and mixing ratios of absorbing gases specified for each layer. If clouds or aerosols are included in the model, their vertical distribution is specified in terms of the aerosol optical depth at a specific reference wavelength, for each particle mode at each layer.

2.9.2 First step – giant exoplanet, brown dwarf or Star

In these cases, we do not have the direct measurements of profile and composition available for Solar system planets. Once again, we start from a pressure–temperature profile for the atmosphere. The other input required for the model is the elemental composition of the atmosphere. For this, we normally assume either a solar composition (e.g. Grevesse, Asplund & Sauval 2007; Asplund et al.

2009; Lodders, Palme & Gail 2009) or a modified solar composition for a different metallicity.

Then for each layer of the atmosphere, we use the ICE chemical equilibrium model (Section 2.1) to determine the equilibrium composition of the layer in terms of molecules, atoms and ions. ICE also predicts what condensates are produced at different levels in the atmosphere, and this can be used as a guide to the addition of clouds to the model which are specified in the same way as in the Solar system case.

Note that VSTAR is not an atmospheric structure model, and so cannot be used to determine structures that are self-consistent with the radiative transfer (although this capability may be added in the future). Currently, therefore, we normally work from a pressure–temperature structure determined from another stellar or exoplanet atmosphere model, and VSTAR is used as a spectral synthesis model.

2.9.3 Second step – computing layer absorption and scattering properties

In either case, we now have a specification of the atmospheric layers with their pressures, temperatures, chemical composition and aerosol optical depth. We now calculate for each layer at each modelled wavelength (typically there are several hundred thousand wavelength points), the absorption and scattering properties. For line absorption, this involves calculating the line profiles of all the spectral lines of all relevant species that fall within the wavelength range of the model (including lines outside the range where the far wing contribution may be significant) and adding their contributions into the gas optical depth of the layer.

For particle scattering (clouds and aerosols – Section 2.7.2), there are two options. Lorenz–Mie theory can be used directly to calculate the scattering properties of each particle mode at each layer for a set of wavelengths. These values are then spline interpolated to provide data for each individual wavelength point. Alternatively, pre-calculated scattering properties can be used and interpolated in the same way.

2.9.4 Third step – radiative transfer solution

The next step is to combine the absorption and scattering properties of each layer as described in Section 2.8 to provide the inputs needed for DISORT, and perform the radiative transfer solution for each wavelength point. At this stage, we specify the boundary conditions, which can include a reflecting surface at the base of the atmosphere, and an illuminating source (the Sun or another star) at a specified zenith angle.

VSTAR can calculate a number of different types of spectra. In the case of a Solar system planet, we are usually interested in the spectrum of the radiance at a specific point on the planet's disc, or the radiance factor (I/F) if we are looking at reflected solar light. For a star, we generally want the flux spectrum (the radiance integrated over all angles) which is equivalent to what would be seen from an unresolved star at a large distance. However, the angular dependence of the radiance also allows the investigation of limb darkening of a star. VSTAR can also calculate the transmission spectrum from the top of the atmosphere to the surface. This is used in particular for the Earth atmosphere case where such data can be used to model telluric corrections to astronomical spectra (Bailey, Simpson & Crisp 2007).

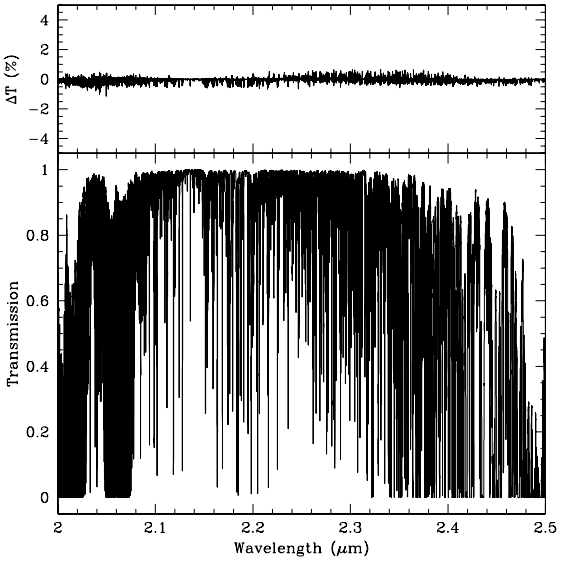

Figure 3. Comparison of Earth atmosphere zenith transmission calculated with VSTAR and RFM in the 2–2.5 μm window. Lower panel: transmission calculated with VSTAR. Upper panel: percentage difference (VSTAR − RFM).

3 TESTS OF VSTAR – COMPARISON WITH OTHER MODELS

We have tested VSTAR by comparing its predictions with a number of other models.

3.1 Comparison with reference forward model

The reference forward model (RFM)[4] is a line-by-line model for the Earth atmosphere developed at Oxford University for the Michelson Interferometer for Passive Atmospheric Sounding (MIPAS) instrument project on the *Envisat* satellite. RFM is itself a development of the earlier GENLN2 model (Edwards 1992). RFM has been included in a number of intercomparison studies of Earth atmosphere radiative transfer codes (Tjemkes et al. 2003; Saunders et al. 2007).

We compared VSTAR with RFM (version 4.25) by using both codes to calculate the Earth atmosphere transmission spectrum at the zenith in the 2–2.5 μm wavelength region. The atmospheric profile was the standard mid-latitude summer atmosphere taken from the RFM website. Absorption due to H_2O, CO_2, O_3, N_2O, CO, CH_4 and O_2 were included in the models with line data taken from the HITRAN 2000 data base (the version of HITRAN supported by RFM).

The transmission spectrum from VSTAR and the percentage difference between transmission calculated by RFM and VSTAR are shown in Fig. 3. The mean difference (VSTAR − RFM) in transmission is −0.05 per cent, and the rms difference is 0.09 per cent. There is no significant trend in the differences with wavelength. These results are basically a test of the line-by-line absorption calculations and show that the two models are in good agreement. Residual differences between the two codes appear to be due to differences in the line shape model used and to differences in the way layer properties are interpolated from the levels listed in the atmospheric profile.

[4] http://www.atm.ox.ac.uk/RFM/

3.2 Radiative transfer benchmarks

We have used VSTAR to reproduce a number of benchmark problems in radiative transfer described by Garcia & Siewert (1985). The first problem considered is a uniform Mie scattering atmosphere containing spherical particles with size parameter 2 and index of refraction 1.33. The atmosphere has a total optical depth $\tau = 1$, and the single scattering albedo $\varpi = 0.95$. The atmosphere is illuminated by a source at a zenith angle of 60° and has a non-reflecting surface at its base. The problem was implemented using VSTAR's own Mie scattering code to calculate the phase function, and the results for the top of atmosphere upward radiances and bottom of atmosphere downward radiances at an azimuth of zero are given in Table 4, and compared with the results summed from the Fourier series coefficients given in Garcia & Siewert (1985). The VSTAR results, calculated with 16 streams in DISORT, agree with the Garcia & Siewert (1985) results to five significant figures in all cases, and at over half the zenith angles agree to within ±1 in the sixth figure. Similar agreement is found for results at other azimuths and optical depths.

Another problem we have calculated with VSTAR is one of the test problems posed by the Radiation Commission of the International Association of Meteorology and Atmospheric Physics (Lenoble 1977). This involves an atmosphere with $\tau = 1$, $\varpi = 0.9$ with a 'Haze L' size distribution of scattering particles as defined by Lenoble (1977). The atmosphere is illuminated by a source at a zenith angle of 60°. This problem has a more complex phase function, and with 16 DISORT streams the benchmark results in Garcia & Siewert (1985) are only matched to an accuracy of ∼1 per cent. However, increasing the number of DISORT streams to 64 produces results that agree with the Garcia & Siewert (1985) results to ±1 in the sixth significant figure for the upward radiances at the top of the atmosphere.

Table 4. Radiances for Mie scattering benchmark problem compared with values from Garcia & Siewert (1985). Positive values of μ are upward radiances at the top of the atmosphere and negative values are downward radiances at the bottom of the atmosphere, both for an azimuth of zero relative to the illuminating source.

$\mu = \cos zd$	VSTAR	Garcia & Siewert	Difference
1.0	0.047 6802	0.047 6807	−0.000 0005
0.9	0.107 2616	0.107 2618	−0.000 0002
0.8	0.162 275	0.162 274	0.000 001
0.7	0.228 132	0.228 131	0.000 001
0.6	0.308 466	0.308 464	0.000 002
0.5	0.406 536	0.406 534	0.000 002
0.4	0.525 328	0.525 326	0.000 002
0.3	0.666 624	0.666 621	0.000 003
0.2	0.828 749	0.828 746	0.000 003
0.1	1.004 042	1.004 041	0.000 001
−0.1	0.466 472	0.466 478	−0.000 006
−0.2	0.578 557	0.578 561	−0.000 004
−0.3	0.653 528	0.653 530	−0.000 002
−0.4	0.682 601	0.682 601	0.000 000
−0.5	0.674 533	0.674 533	0.000 000
−0.6	0.637 904	0.637 903	0.000 001
−0.7	0.578 009	0.578 008	0.000 001
−0.8	0.496 937	0.496 936	0.000 001
−0.9	0.391 880	0.391 879	0.000 001
−1.0	0.197 933	0.197 932	0.000 001

3.3 Comparison with MARCS

The MARCS stellar atmosphere code (Gustafsson et al. 2008) is a good choice for a comparison with VSTAR, since it uses modern abundances and opacities, similar to those used in VSTAR, and has been used to generate a large grid of model atmospheres with detailed information available on the model structure. The comparison shown here is for a plane-parallel model with $T_{\rm eff} = 2500$ K, $g = 1000\,{\rm m\,s^{-2}}$ ($\log g = 5$ in cgs units) and solar metallicity. To make the comparison, we take the temperature as a function of gas pressure from the MARCS model, and use this as the input for calculating an equivalent VSTAR model.

Molecular species included in the VSTAR model were H_2O (BT2), CO, CaH, MgH, FeH, CrH, TiO and VO. Lines of alkali metals were taken from VALD (Piskunov et al. 1995; Kupka et al. 1999), and other atomic species were from the Kurucz line lists.

Fig. 4 shows some comparisons of data from MARCS and VSTAR. These include the height above the lowest level modelled (determined from hydrostatic balance) and the mixing ratios of several important species. On these plots, crosses are the values from MARCS and the lines are the values from VSTAR. In most cases, the agreement is excellent. The behaviour for TiO is, however, quite different in the cooler layers. This is because the VSTAR chemical model includes condensate formation, whereas MARCS only includes gas-phase chemistry. Small differences in the CO and H_2O mixing ratios arise from the same cause. The difference in TiO does not have much effect on the strength of the TiO bands in the spectrum as these are mostly formed at deeper levels.

The flux spectrum from VSTAR is compared with that from MARCS in the bottom right-hand panel of Fig. 4. The fluxes provided with MARCS are described as 'rough estimates of the surface fluxes' and 'are *not* synthetic spectra'. Nevertheless, it is clear that the values of the fluxes are very similar and the same absorption features are present in both spectra at similar depths. A comparison of similar models with observations of an M dwarf spectrum is presented later.

4 COMPARISON WITH OBSERVATIONS

In this section, we present a brief comparison of VSTAR models with observed spectra for a range of objects. Full details on these and other results will be given elsewhere, but they are presented here to show the wide range of astronomical objects that can be successfully modelled using VSTAR. The spectra of Solar system objects are from our own observations with the Anglo-Australian 3.9-m telescope at Siding Spring Observatory, and its Infrared Imager Spectrometer 2 (IRIS2) instrument (Tinney et al. 2004), and from the Near-Infrared Integral Field Spectrometer (NIFS) instrument (McGregor et al. 2003) on the Gemini North 8-m telescope at Mauna Kea, Hawaii. The brown dwarf and stellar spectra are taken from the NASA Infrared Telescope Facility (IRTF) spectral library (Cushing, Rayner & Vacca 2005; Rayner, Cushing & Vacca 2009) and are taken with the SpeX instrument on IRTF at a resolving power of $R \sim 2000$.

The spectra considered here are all in the near-IR spectral region (1–2.5 μm). For late-type dwarfs, this is where the flux peaks, and for spectroscopy of planets, this is a region containing many interesting rovibrational molecular bands. While this is the wavelength region VSTAR has normally been applied to, there is nothing inherent in VSTAR that restricts it to this region. VSTAR should, in principle, be usable from UV to microwave wavelengths.

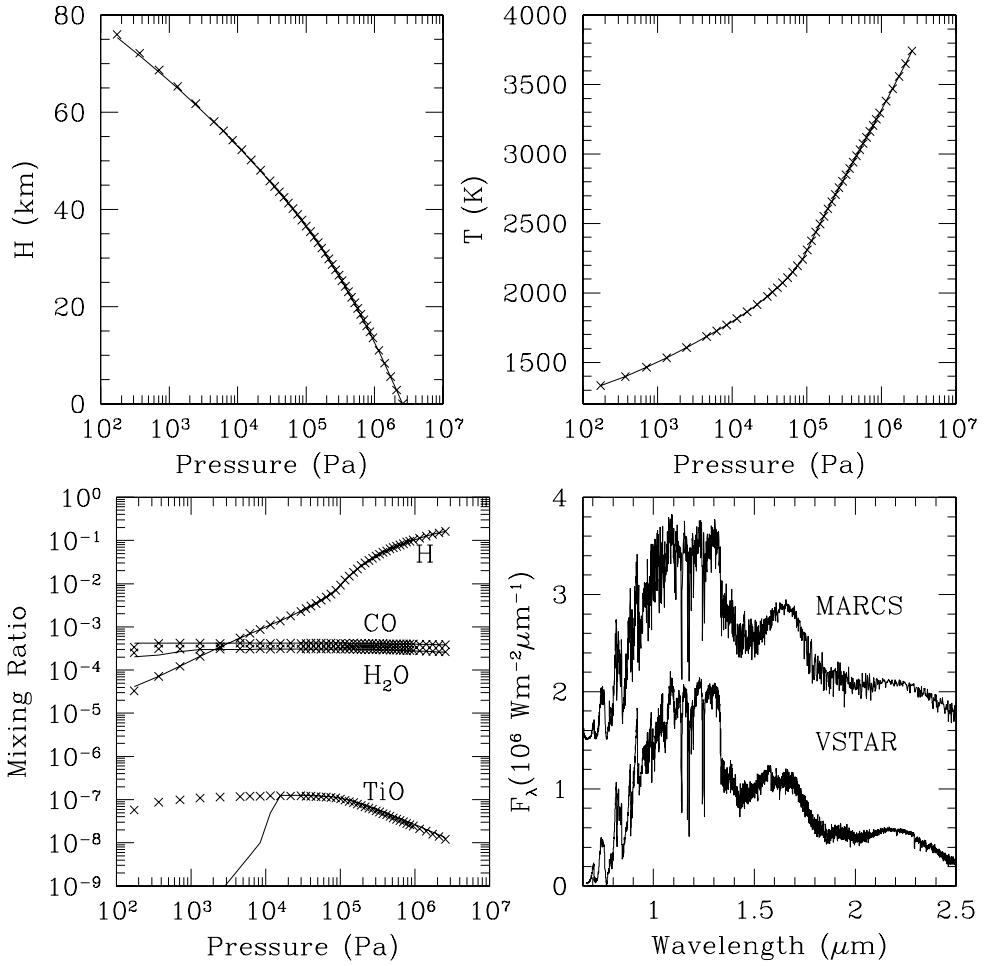

Figure 4. Comparison of MARCS and VSTAR for a stellar atmosphere model with $T_{\rm eff} = 2500$ K, $\log g = 5$ and solar metallicity. The height, temperature and mixing ratios of several important species are plotted as a function of gas pressure. On these plots, crosses are the values from MARCS, and the line shows the values from VSTAR. (Only the temperature profile is taken from the MARCS model. All other quantities are calculated independently by VSTAR and MARCS.) The flux spectra from MARCS and VSTAR are shown in the bottom right-hand panel, with the MARCS data offset by 1.5×10^6.

4.1 Solar system objects

Fig. 5 shows a number of comparisons of observed spectra with VSTAR models for Solar system atmospheres. The Earth atmosphere transmission comparison (top left-hand panel) is described in more detail in Bailey et al. (2007, 2008b) and uses the observed spectrum at a resolving power of $R\,(=\lambda/\Delta\lambda) \sim 2400$ of the G5V star BS 996 with the 3.9-m Anglo-Australian Telescope (AAT) and its IRIS2 instrument. This spectrum is compared with a model of a solar spectrum as seen through a modelled Earth atmosphere transmission spectrum calculated using VSTAR. Of the spectral features, only that near 1.28 μm is a stellar line. Other features are atmospheric absorptions of O_2, CO_2 and H_2O, with the strongest feature being the O_2 $a - X$ band at 1.27 μm and its associated CIA. The data and model agree to better than 1 per cent.

The bottom left-hand panel shows the reflected light spectrum of Jupiter in the near-IR K band (2.04–2.38 μm), also observed with the AAT and IRIS2. The VSTAR model used here is described in more detail in Kedziora-Chudczer & Bailey (2011). The absorption features present in this spectral region are due to methane, and to the CIA of H_2–H_2 (see Section 2.6.2), with the latter producing the broad smooth feature centred on 2.11 μm. Stratospheric and tropospheric clouds are included in the model with the details of the cloud properties and optical depths given in Kedziora-Chudczer & Bailey (2011).

The right-hand panels of Fig. 5 show spectra of Titan and Uranus in the spectral region covering the 1.55-μm methane 'window' that lies between strong methane absorption bands. Modelling of the spectra of these objects at this wavelength using line-by-line methods has only become possible very recently with the availability of the latest laboratory spectral line data for methane as described in Section 2.2.6, in particular the data of Wang et al. (2011). The Titan spectrum was obtained with the NIFS on the Gemini North 8-m telescope, and the data and VSTAR model are described more fully by Bailey et al. (2011). The absorption lines in this region are mostly weak lines of CH_4, but there are also lines of CH_3D and CO. A model for Titan's aerosols based on that of Tomasko et al. (2008) is also used in this analysis. The models enabled Titan's D/H ratio and CO abundance to be determined as described in Bailey et al. (2011).

The Uranus comparison in the lower right-hand panel uses data from IRIS2 on the AAT. The VSTAR model spectrum is calculated from the new low-temperature methane line data as described in Section 2.2.6. The model includes clouds with a mean particle size

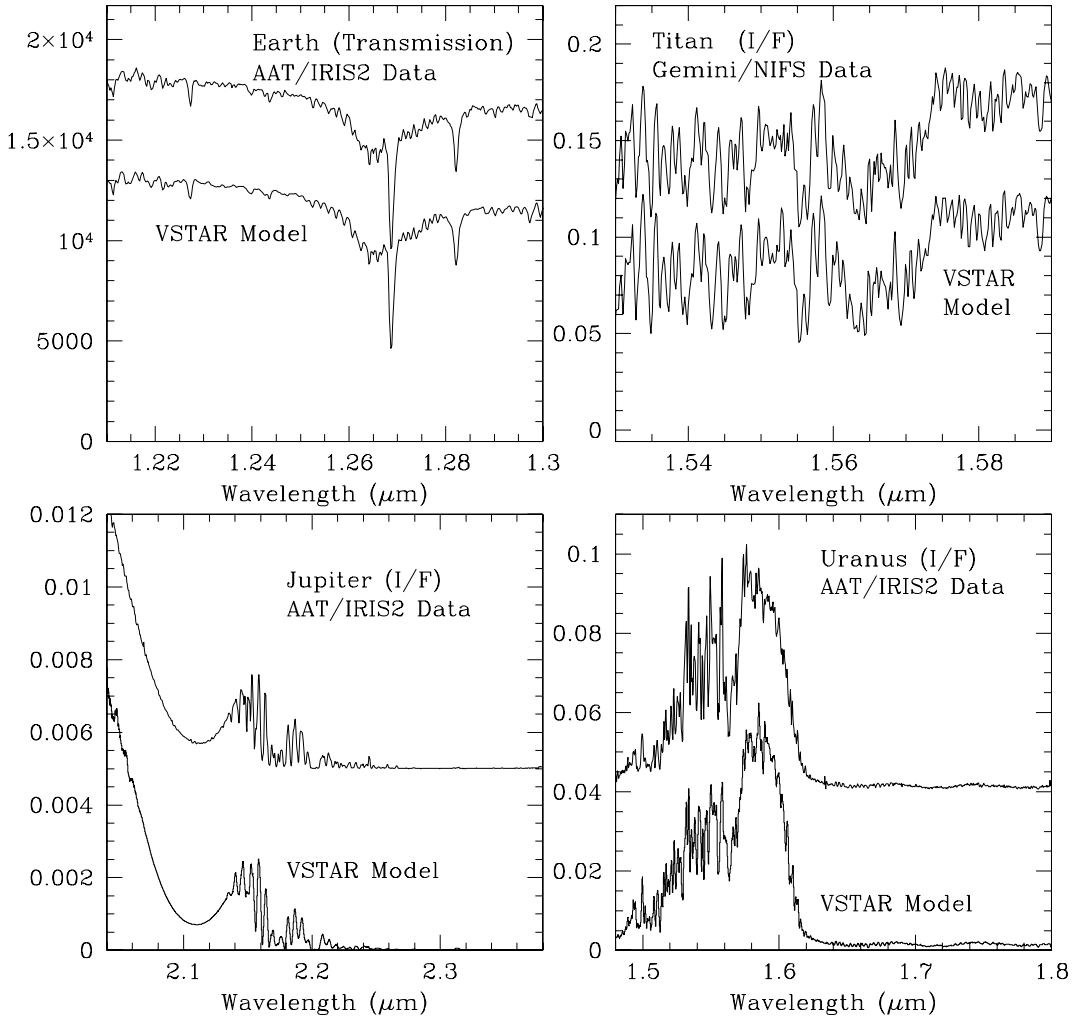

Figure 5. Comparison of observed spectrum of Solar system objects with VSTAR model spectra. At top left is shown the spectrum of a G2V star seen through the Earth's atmosphere in the region of the O_2 $a - X$ absorption band, compared with a VSTAR model for a solar spectrum with Earth atmospheric transmission applied. The other three panels show observed reflectance spectra of Titan, Jupiter and Uranus compared with VSTAR models. The observed spectrum in each case is offset upwards relative to the model spectrum.

of 1 μm, and with the main cloud layers being at 2–3 and 6–10 bar, which is similar to cloud distributions derived by Sromovsky, Irwin & Fry (2006) and Irwin, Teanby & Davis (2007).

While not shown here, VSTAR has also been used successfully to model the spectra of other Solar system planets. VSTAR models for the Venus night side are used in the analyses described by Bailey (2009) and Cotton et al. (2011).

4.2 Brown dwarf

Fig. 6 shows an observed spectrum of the T4.5 dwarf 2MASS J05591915−1404489 taken from the IRTF spectral library (Cushing et al. 2005; Rayner et al. 2009) compared with a VSTAR model spectrum. The VSTAR spectra used for this comparison are based on brown dwarf model P–T structures taken from figs 8 and 9 of Burrows et al. (2006). The VSTAR models included molecular absorption due to H_2O (BT2), CO, CH_4, CaH, MgH, CrH, FeH and TiH. Lines of alkali metals are included from VALD (Piskunov et al. 1995; Kupka et al. 1999). The far wings of very strong sodium and potassium lines in the visible have a significant effect on the shape of brown dwarf spectra in the 1-μm region. We used a χ factor model for the far wing shapes of these lines with an exponential decrease between 500 and 7500 cm^{-1} from the line centre, with the parameters adjusted to provide a good match to the data. More physically based models for the far wing shapes of alkali metal lines are described by Burrows & Volobuyev (2003) and Allard et al. (2003).

A number of models were tried with different temperatures and gravities, and best agreement with the data was found for a model with $T_{\rm eff} = 1100$ K, $g = 1000$ m s^{-2} ($\log g = 5$ in cgs units) and solar metallicity. This is in reasonable agreement with other results for this object. Stephens et al. (2009) find $T_{\rm eff} = 1200$ K, $\log g = 4.5$, while del Burgo et al. (2009) find $T_{\rm eff} = 1002$ K, $\log g = 4.9$ using high-resolution spectra.

The model spectrum agrees well with the observed spectrum except in the wavelength region from around 1.6 to 1.7 μm. As discussed in Section 2.2.6, the methane line lists currently available do not include hot bands in this region and therefore underestimate the total absorption, and incorrectly model the observed structure. This problem exists with all models for T dwarf spectra. There is also a discrepancy between the model and observations in the 2.1-μm region where the model is slightly too low.

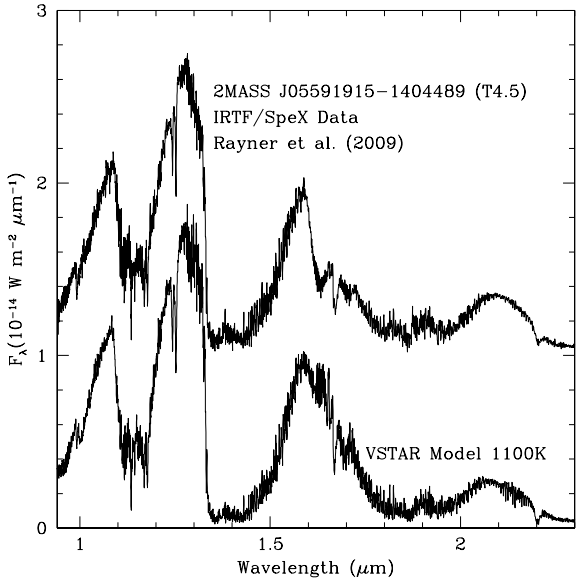

Figure 6. Comparison of observed spectrum of the T4.5 dwarf 2MASS J055591915−1404489 with a model spectrum calculated with VSTAR for $T_{\rm eff} = 1100$ K and $\log g = 5$. The observed spectrum is offset from the model upwards by 1 ($\times 10^{-14}$).

In other wavelength regions, where methane absorption is not significant, the agreement between model and observations is excellent. What might, at first sight, appear to be noise on the spectra is in fact spectral structure due to many absorption lines. This is apparent from Fig. 7 where two wavelength regions (1.1–1.27 and 1.4–1.58 μm) are shown on an expanded scale.

The model used here did not include dust absorption and scattering. This is acceptable for objects as late as T4.5. For earlier-type brown dwarfs, and in particular the L dwarf class, the effects of dust are important. While VSTAR is quite capable of modelling the radiative effects of dust in such systems, there are currently considerable differences in the assumptions about dust properties used in different models. Some models use large (∼100 μm) dust particles (Burrows et al. 2006), while others use small (sub-μm) particles (Allard et al. 2001). For the purposes of this paper, we have avoided the extra complexity of dusty brown dwarf models.

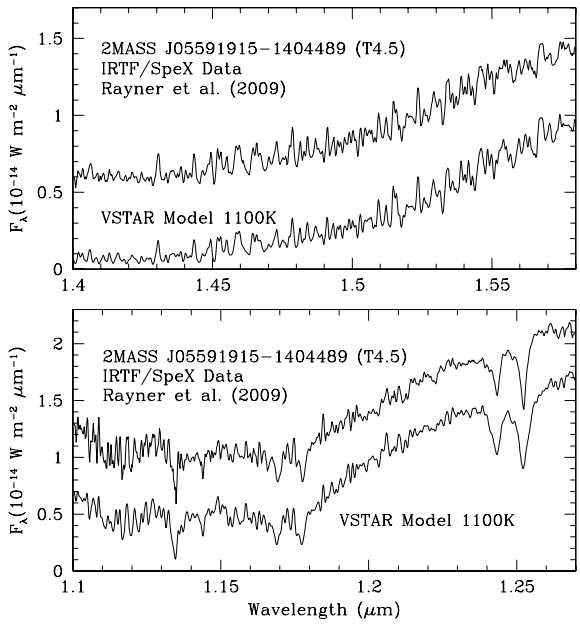

Figure 7. Expanded view of two sections of the spectrum shown in Fig. 6. The observed spectra are offset from the model upwards by 0.5 ($\times 10^{-14}$).

Our models also assume equilibrium chemistry. Some brown dwarf models include a non-equilibrium treatment of the chemistry of some species such as CH_4, CO and H_2O (Saumon et al. 2003; Stephens et al. 2009) which allows for the effects of vertical mixing in the atmosphere. While this could be implemented as a modification to our chemical model, we have not done so for the results presented here. The effects on the near-IR spectrum appear to be small (Hubeny & Burrows 2007), with more significant effects at 4–14 μm wavelengths.

4.3 M dwarf

Fig. 8 shows an observed spectrum of the M8 dwarf VB 10 (Gl 752B) taken from the IRTF spectral library (Cushing et al. 2005; Rayner et al. 2009) compared with a model spectrum calculated with VSTAR. The model structure was taken from the MARCS grid of model atmospheres (Gustafsson et al. 2008) and is a model for $T_{\rm eff} = 2700$ K, $g = 1000\,{\rm m\,s^{-2}}$ ($\log g = 5$ in cgs units) and solar metallicity. In other respects, the model is similar to that described in Section 3.3. A number of different effective temperatures were tested with the 2700-K model providing the best match to the observed spectrum.

Fig. 9 shows expanded views of two regions of the spectrum. The upper panel shows the 1.58–1.78 μm region. This is dominated by absorption lines in the $E - A$ band of FeH which are included in our model using the line list of Hargreaves et al. (2010). This band is essential to get a good model of the spectrum in this region. However, including this line list results in a small step in the modelled spectrum at 1.582 μm (visible in Fig. 8) which is the shortest wavelength included in this list. This step is not seen in the observed spectrum, and suggests that there is more FeH absorption at shorter wavelengths that should be included. The lower panel of

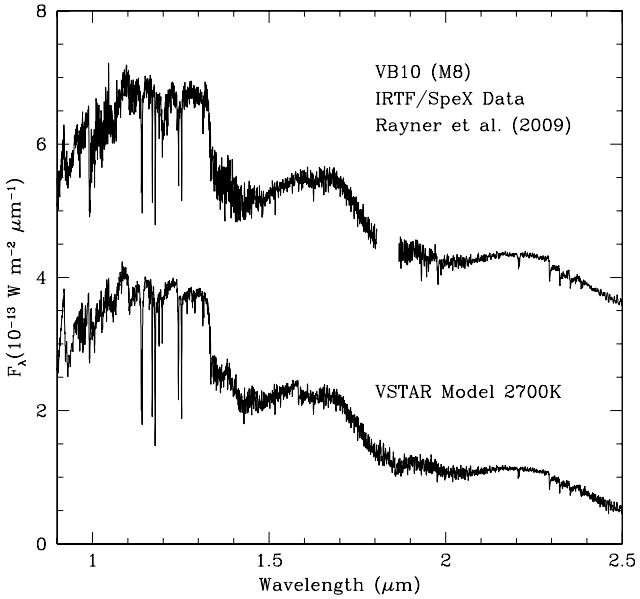

Figure 8. Comparison of observed spectrum of the M8 dwarf VB 10 with a model spectrum calculated with VSTAR using a MARCS model structure for $T_{\rm eff} = 2700$ K and $\log g = 5$. The observed spectrum is offset from the model upwards by 3 ($\times 10^{-13}$).

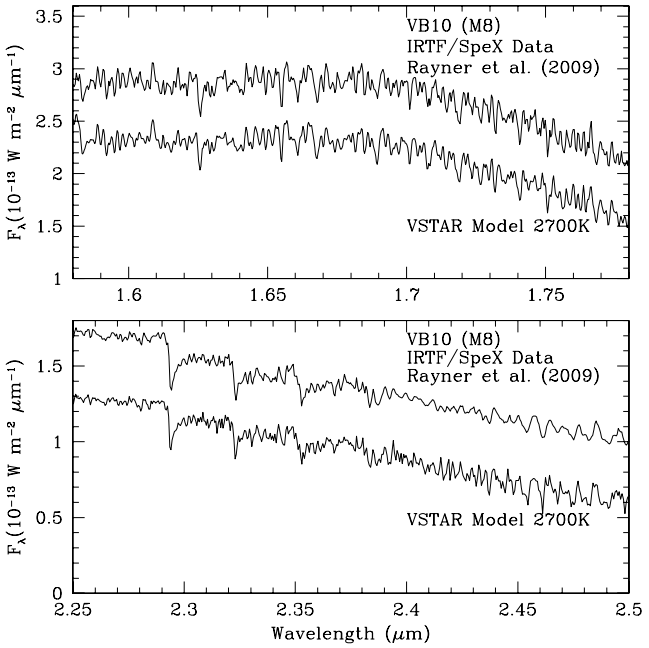

Figure 9. Expanded view of two sections of the spectrum shown in Fig. 8. The observed spectra are offset from the model upwards by 0.4 ($\times 10^{-13}$). The upper panel shows primarily absorption in the E-A band of FeH. The lower panel shows absorption due to CO and H_2O.

Fig. 9 shows the 2.25–2.5 μm region; it shows that the model does a good job of representing the detailed structure of the CO and H_2O bands in this region. As for the brown dwarf case, we have used a dust-free model. It is quite possible that dust is present in such a late-type M dwarf, and its inclusion might change our conclusions about the best-fitting effective temperature.

The upper limit on the layer temperature for modelling stellar atmospheres using VSTAR is currently 6000 K set by the use of data from the JANAF tables in our chemical model. Since a model usually requires a range of layer temperatures extending to about a factor of 2 above and below the effective temperature of the star being modelled, the maximum effective temperature is around 3000 K.

5 CONCLUSIONS

We have described the techniques used in the VSTAR code to calculate model spectra for objects including Solar system planets, brown dwarfs and M dwarfs. While there are other codes used for modelling the spectra of these objects, VSTAR has a number of unique features.

(i) It is capable of being used for a very wide range of objects, ranging from the coolest Solar system planets (Uranus with layer temperatures down to 60 K) to stars with layer temperatures up to 6000 K.

(ii) It has been tested by comparison with both the Earth atmosphere radiative transfer code (RFM) and a stellar atmosphere code (MARCS).

(iii) Not only is a rigorous approach to radiative transfer used, but this has also been tested against radiative transfer benchmarks and shown to be accurate to levels of 10^{-5} to 10^{-6}.

An obvious application of VSTAR is to the modelling of exoplanet spectra. VSTAR has the proven ability to model both cool planets in our own Solar system and hotter objects such as brown dwarfs and M dwarfs, and thus covers the full temperature range expected to be encountered in exoplanets. The full treatment of the angular dependence of scattering incorporated in VSTAR means that it can be used to predict the phase dependence of an exoplanet spectrum around its orbital cycle.

Work is currently in progress on extending VSTAR to include polarized radiative transfer. The phase variation of polarization can potentially provide important information about an exoplanet's atmosphere or surface (Bailey 2007; Stam 2008; Zugger et al. 2010)

ACKNOWLEDGMENTS

Based on observations obtained at the Gemini Observatory which is operated by the Association of Universities for Research in Astronomy, Inc. under a cooperative agreement with the NSF on behalf of the Gemini partnership: the National Science Foundation (United States), the Science and Technology Facilities Council (United Kingdom), the National Research Council (Canada), CONICYT (Chile), the Australian Research Council (Australia), Ministerio da Cienca e Tecnologia (Brazil) and Ministerio de Ciencia, Tecnologia e Innovacion Productiva (Argentina). The Titan observations were obtained as part of the system verification of the NIFS instrument under programme GN-2006A-SV-128. We thank the staff of the Australian Astronomical Observatory for assistance in obtaining observations with the Anglo-Australian Telescope.

REFERENCES

Albert S., Bauerecker S., Boudon V., Brown L. R., Champion J.-P., Loete M., Nikitin A., Quack M., 2009, Chem. Phys., 356, 131
Allard F., Hauschildt P. H., Schwenke D., 2000, ApJ, 540, 1005
Allard F., Hauschildt P. H., Alexander D. R., Tamanai A., Schweitzer A., 2001, ApJ, 556, 357
Allard N. F., Allard F., Hauschildt P. H., Kielkopf J. F., Machin L., 2003, A&A, 411, 473
Asplund M., Grevesse N., Sauval A. J., Scott P., 2009, ARA&A, 47, 481
Bailey J., 2006, in Forget F. et al., eds, Proc. Workshop on Mars Atmosphere Modelling and Observations. Laboratoire Meteorologie Dynamique, Paris, 148
Bailey J., 2007, Astrobiology, 7, 320
Bailey J., 2009, Icarus, 201, 444
Bailey J., Simpson A., Crisp D., 2007, PASP, 119, 228
Bailey J., Ulanowski Z., Lucas P. W., Hough J. H., Hirst E., Tamura M., 2008a, MNRAS, 386, 1016
Bailey J., Meadows V. S., Chamberlain S., Crisp D., 2008b, Icarus, 197, 247
Bailey J., Ahlsved L., Meadows V. S., 2011, Icarus, 213, 218
Barber R. J., Tennyson J., Harris G. J., Tolchenov R. N., 2006, MNRAS, 368, 1087
Barin I., 1995, Thermochemical Data of Pure Substances, 3rd edn. VCH-Verlag, Weinheim
Barman T. S., Hauschildt P. H., Allard F., 2001, ApJ, 556, 885
Bell K. L., 1980, J. Phys. B, 13, 1859
Bell K. L., Berrington K. A., 1987, J. Phys. B, 20, 801
Borysov A., Champion J. P., Jørgensen U. G., Wenger C., 2002, Molecular Phys., 100, 3585
Borysow A., 2002, A&A, 390, 779
Borysow A., Frommhold L., 1989, ApJ, 341, 549
Borysow A., Frommhold L., Massimo M., 1989, ApJ, 336, 495
Borysow A., Jørgensen U. G., Zheng C., 1997, A&A, 324, 185
Borysow A., Jørgensen U. G., Fu Y., 2001, J. Quant. Spectrosc. Radiative Transfer, 68, 235
Boudon V., Rey M., Loete M., 2006, J. Quant. Spectrosc. Radiative Transfer, 98, 394
Brown L. R., 2005, J. Quant. Spectrosc. Radiative Transfer, 96, 251
Brown L. R., Peterson D. B., 1994, J. Molecular Spectrsoc., 168, 593

Burch D. E., Singleton E. B., Williams D., 1962, Applied Opt., 1, 359
Burch D. E., Gryvnak D. A., Patty R. R., Bartky C. E., 1969, J. Opt. Soc. Am., 59, 267
Burrows A., Sharp C. M., 1999, ApJ, 512, 843
Burrows A., Volobuyev M., 2003, ApJ, 583, 985
Burrows A., Ram R. S., Bernath P., Sharp C. M., Milsom J. A., 2002, ApJ, 577, 986
Burrows A., Sudarsky D., Hubeny I., 2003, ApJ, 588, 1121
Burrows A., Dulick M., Bauschlicher C. W., Bernath P. F., Ram R. S., Sharp C. M., Milson J. A., 2005, ApJ, 624, 988
Burrows A., Sudarsky D., Hubeny I., 2006, ApJ, 640, 1063
Cahoy K. L., Marley M. S., Fortney J. J., 2010, ApJ, 724, 189
Campargue A., Wang L. Kassi S., Masát M., Ondřej. V., 2010, J. Quant. Spectrosc. Radiative Transfer, 111, 1141
Chandrasekhar S., 1960, Radiative Transfer. Dover, New York
Chase M. W., 1998, J. Phys. Chem. Ref. Data Monograph No. 9, NIST-JANAF Thermochemical Tables. American Chemical Society. Am. Inst. Phys., Woodbury
Cotton D. V., Bailey J., Crisp D., Meadows V. S., 2011, Icarus, doi: 10.1016/j.icarus.2011.05.020
Cox A. N., 2000, Allen's Astrophysical Quantities, 4th edn. Springer-Verlag, New York
Cushing M. C., Rayner J. T., Vacca W. D., 2005, ApJ, 623, 1115
Cushing M. C. et al., 2006, ApJ, 648, 614
Dalgarno A., Williams D. A., 1962, ApJ, 136, 690
de Bergh C. et al., 2011, Planet. Space Sci., in press (doi:10.1016/j.pss.2011.05.003)
del Burgo C., Martin E. L., Zapatero Osorio M. R., Hauschildt P. H., 2009, A&A, 501, 1059
Delaye C., Hartmann J.-M., Taine J., 1989, Applied Opt., 28, 5080
Dulick M., Bauschlicher C. W., Burrows A., Sharp C. M., Ram R. S., Bernath P., 2003, ApJ, 594, 651
Edwards D. P., 1992, NCAR Technical Note NCAR/TN-367+STR, National Centre for Atmospheric Research, Boulder, Colorado
Fischer J., Gamache R. R., Goldman A., Rothman L. S., Perrin A., 2003, J. Quant. Spectrosc. Radiative Transfer, 82, 401
Fortney J. J., Marley M. S., Lodders K., Saumon D., Freedman R., 2005, ApJ, 627, L69
Freedman R. S., Marley M. S., Lodders K., 2008, ApJS, 174, 504
Gamache R. R., Lynch R., Brown L. R., 1996, J. Quant. Spectrosc. Radiative Transfer, 56, 471
Gao B., Kassi S., Campargue A., 2009, J. Molecular Spectrosc., 253, 55
Garcia R. D. M., Siewert C. E., 1985, Transport Theory Statistical Phys., 14, 437
Goody R., West R., Chen L., Crisp D., 1989, J. Quant. Spetrosc. Radiative Transfer, 42, 539
Goorvitch D., 1994, ApJS, 95, 535
Gray D. F., 2005, The Observation and Analysis of Stellar Photospheres, 3rd edn. Cambridge Univ. Press, Cambridge
Grevesse N., Asplund M., Sauval A. J., 2007, Space Sci. Rev., 130, 115
Gustaffson B., Edvadrsson B., Eriksson K., Jørgensen U. G., Nordlund A., Plez B., 2008, A&A, 486, 951
Hansen J. E., Travis L. D., 1974, Space Sci. Rev., 16, 527
Hargreaves R. J., Hinkle K. H., Bauschlicher C. W., Wende S., Seifahrt A., Bernath P. F., 2010, AJ, 140, 919
Harris G. J., Tennyson J., Kaminsky B. M., Pavlenko, Ya. V., Jones H. R. A., 2006, MNRAS, 367, 400
Hartmann J. M., Rosenmann L., Perrin M. Y., Taine J., 1988, Applied Opt., 27, 3063
Henyey L. G., Greenstein J. L., 1941, ApJ, 93, 70
Homeier D., Hauschildt P. H., Allard F., 2003, in Hubeny I., Mihalas D., Werner K., eds, ASP Conf. Ser. Vol. 288, Stellar Atmosphere Modelling. Astron. Soc. Pac., San Francisco, p. 357
Hubeny I., Burrows A., 2007, ApJ, 669, 1248
Humlicek J., 1982, J. Quant. Spectrosc. Radiative Transfer, 27, 437
Irwin A. W., 1981, ApJS, 45, 621
Irwin A. W., 1988, A&AS, 74, 145
Irwin P. G. J., Sromovsky L. A., Strong E. K., Sihra K., Teanby N. A., Bowles N., Calcutt S. B., Remedios J. J., 2006, Icarus, 181, 309
Irwin P. G. J., Teanby N. A., Davis G. R., 2007, ApJ, 665, L71
Jacquinet-Husson N. et al., 2008, J. Quant. Spectrosc. Radiative Transfer, 109, 1043
Jones H. R. A., Pavlenko Y., Viti S., Tennyson J., 2003, in Brown A., Harper G. M., Ayres T. R., eds, The Future of Cool-Star Astrophysics: 12th Cambridge Workshop on Cool Stars, Stellar Systems, and the Sun. Univ. of Colorado, Boulder, p. 899
Jørgensen U. G., 1994, A&A, 284, 179
Jørgensen U. G., Larsson M., 1990, A&A, 238, 424
Jørgensen U. G., Larsson M., Iwamae A., Yu B., 1996, A&A, 315, 204
Jørgensen U. G., Jensen P., Sørensen G. O., Aringer B., 2001, A&A, 372, 249
Karkoschka E., Tomasko M. G., 2010, Icarus, 205, 674
Kedziora-Chudczer L., Bailey J., 2011, MNRAS, 414, 1483
Kupka F., Piskunov N., Ryabchiokva T. A., Stempels H. C., Weiss W. W., 1999, A&AS, 138, 119
Kurucz R., 1970, SAO Special Report 309, Atlas: a Computer Program for Calculating Model Stellar Atmospheres. Smithsonian Astrophysical Observatory, Cambridge, MA
Kurucz R., 2005, Mem. Soc. Astron. Ital. Suppl. 8, 86
Kurucz R., Avrett E. H., 1981, SAO Special Report 391, Solar Spectrum Synthesis I. A Sample Atlas from 224 to 300nm. Smithsonian Astrophysical Observatory, Cambridge, MA
Laraia A. L., Gamache R. R., Lamouroux J., Gordon I. E., Rothman L. S., 2011, Icarus, 215, 391
Lenoble J., ed., Standard Procedures to Compute Atmospheric Radiative Transfer. National Centre for Atmospheric Research, Boulder, Colorado
Liou K. N., 2002, An Introduction to Atmospheric Radiation. Academic Press, San Diego
Lodders K., 1999, J. Phys. Chemical Reference Data, 28, 1705
Lodders K., 2004, J. Phys. Chemical Reference Data, 33. 357
Lodders K., Fegley B., 2002, Icarus, 155, 393
Lodders K., Palme H., Gail H.-P., 2009, preprint (arXiv:1001.4635)
McGregor P. J. et al., 2003, Proc. SPIE, 4841, 1551
McKay C. P., Pollack J. B., Courtin R., 1989, Icarus, 80, 23
McKellar A. R. W., 1989, Icarus, 80, 361
Marcy G. W., Butler R. P., Williams E., Bildsten L., Graham J. R., Ghez A. M., Jernigan J. G., 1997, ApJ, 481, 926
Margolis J. S., 1990, Applied Opt., 29, 2295
Marley M. S., McKay, 1999, Icarus, 138, 268
Marley M. S., Seager S., Saumon D., Lodders K., Ackerman A. S., Freedman R. S., Fan X., 2002, ApJ, 568, 335
Mayer J. E., Mayer M. G., 1940, Statistical Mechanics. Wiley, New York
Mayor M., Queloz D., 1995, Nat, 378, 355
Meadows V. S., Crisp D., 1996, J. Geophys. Res., 101, 4595
Mishchenko M. I., 1991, J. Opt. Soc. Am., 8, 871
Mishchenko M. I., Travis L. D., Lacis A. A., 2002, Scattering, Absorption and Emission of Light by Small Particles. Cambridge Univ. Press, Cambridge
Mondelain D., Kassi S., Wang L., Campargue A., 2011, Phys. Chem. Chem. Phys., 13, 7985
Nakajima T., Oppenheimer B. R., Kulkarni S. R., Golimowski D. A., Matthews K., Durrance S. T., 1995, Nat, 378, 463
Nikitin A. V. et al., 2010, J. Quant. Spectrosc. Radiative Transfer, 111, 2211
Nikitin A. V. et al., 2011, J. Quant. Spectrosc. Radiative Transfer, 112, 28
Nouri S., Orphal J., Aroui H., Hartmann J.-M., 2004, J. Molecular Spectrosc., 227, 60
Old J. G., Gentili K. L., Peck E. R., 1971, J. Opt. Soc. A., 61, 89
Oppenheimer B. R., Kulkarni S. R., Matthews K., Nakajima T., 1995, Sci, 270, 1478
Partridge H., Schwenke D. W., 1997, J. Chem. Phys., 106, 4618
Pavlenko Ya. V., Jones H. R. A., Lyubchik, Yu., Tennyson J., Pinfield D. J., 2006, A&A, 447, 709
Peck E. R., Reeder K., 1972, J. Opt. Soc. Am., 62, 950

Perrin M. Y., Hartmann J. M., 1989, J. Quant. Spectrosc. Radiative Transfer, 42, 311
Pine A. S., 1992, J. Chem. Phys., 97, 773
Pine A. S., Gabard T., 2003, J. Molecular Spectrosc., 217, 105
Piskunov N. E., Kukpa F., Ryabchikova T. A., Weiss W. W., Jeffery C. S., 1995, A&AS, 112, 525
Plez B., 1998, A&A, 337, 495
Pollack J. B. et al., 1993, Icarus, 103, 1
Querci F., Querci M., Kunde V. G., 1971, A&A, 15, 256
Querci F., Querci M., Tsuji T., 1974, A&A, 31, 265
Rayner, J.T., Cushing, M.C., Vacca, W.D., 2009, ApJS, 185, 289
Régalia-Jarlot L., Thomas X., Von der Heyden P., Barbe A., 2005, J. Quant. Spectrosc. Radiative Transfer, 91, 121
Robert O., Hilico J.-C., Loete M., Champion J.-P., Brown L. R., 2001, J. Molecular Spectrosc., 209, 14
Robie R. A., Hemingway B. S., 1995, US Geological Survey Bull. 2131
Rothman L. S., Wattson R. B., Gamache R., Schroeder J. W., McAnn A., 1995, in Daintey J. C., ed., Proc. SPIE Conf. Ser. Vol. 2471, Atmospheric Propagation and Remote Sensing IV. SPIE, Bellingham, p. 105
Rothman L. S. et al., 1998, J. Quant. Spectrosc. Radiative Transfer, 60, 665
Rothman L. S. et al., 2005, J. Quant. Spectrosc. Radiative Transfer, 96, 139
Rothman L. S. et al., 2009, J. Quant. Spectrosc. Radiative Transfer, 110, 533
Rothman L. S. et al., 2010, J. Quant. Spectrosc. Radiative Transfer, 111, 2139
Saumon D., Marley M. S., Lodders K., Freedman R. S., 2003, in Martin E. L., ed., Proc. IAU Symp. 211, 'Brown Dwarfs'. Astron. Soc. Pac., San Francisco, p. 345
Saunders R. et al., 2007, J. Geophys. Res., 112, D01S90
Sauval A. J., Tatum J. B., 1984, ApJS, 56, 193
Schreier F., 1992, J. Quant. Spectrosc. Radiative Transfer, 27, 437
Schwenke D., 1998, Faraday Discussions, 109, 321
Schwenke D., Partridge H., 2000, J. Chem. Phys., 113, 129
Seager S., Whitney B. A., Sasselov D. D., 2000, ApJ, 540, 504
Seiff A. et al., 1985, Advances Space Res., 5, 3
Sharp C. M., Burrows A., 2007, ApJS, 168, 140
Sharp C. M., Huebner W. F., 1990, ApJ, 72, 417
Šimečková M., Jacquemart D., Rothman L. S., Gamache R. R., Goldman A., 2006, J. Quant. Spectrosc. Radiative Transfer, 98, 130
Skory S., Weck P. F., Stancil P. C., Kirby K., 2003, ApJS, 148, 599
Smith K. M., Newnham D. A., 1999, Chemical Phys. Lett., 308, 1
Smith K. M., Newnham D. A., 2000, J. Geophys. Res., 105, D6, 7383
Sneep M., Ubachs W., 2005, J. Quant. Spectrosc. Radiative Transfer, 92, 293
Sromovsky L. A., Irwin P. G. J., Fry P. M., 2006, Icarus, 182, 577
Stam D. M., 2008, A&A, 482, 989
Stamnes K., Tsay S. C., Wiscombe W., Jayaweera K., 1988, Applied Opt., 27, 2502
Stephens D. C. et al., 2009, ApJ, 702, 154
Strong K., Taylor F. W., Calcutt S. B., Remedios J. J., Ballard J., 1993, J. Quant. Spectrosc. Radiative Transfer, 50, 363
Swain M. R., Vasisht G., Tinnetti G., 2008, Nat, 452, 329
Swain M. R., Vasisht G., Tinetti G., Bouwman J., Chen, p., Yung Y., Deming D., Deroo P., 2009a, ApJ, 690, L114
Swain M. R. et al., 2009b, ApJ, 704, 1616
Tashkun S. A., Perevalov V. I., Teffo, J-L., Bykov A. D., Lavrentieva N. N., 2003, J. Quant. Spectrosc. Radiative Transfer, 82, 165
Tinney C. et al., 2004, Proc. SPIE, 5492, 998
Tjemkes S. A. et al., 2003, J. Quant. Spectrosc. Radiative Transfer, 77, 433
Tomasko M. G., Doose L., Engel S., Dafoe L. E., West R., Lemmon M., Karkoschka E., See C., 2008, Planet. Space Sci., 56, 669
Tonkov M. V. et al., 1996, Applied Opt., 35, 4863
Tsuji T., 1973, A&A, 23, 411
Tsuji T., Ohnaka K., Aoki W., Nakajima T., 1996, A&A, 308, L29
van Vleck J. H., Weisskopf V. F., 1945, Rev. Modern Phys., 17, 227
Vidler M., Tennyson J., 2000, J. Phys. Chem., 113, 9766
Voronin B. A., Tennyson J., Tolchenov R. N., Lugovskoy A. A., Yurchenko S. N., 2010, MNRAS, 402, 492
Wang L., Kassi S., Campargue A., 2010, J. Quant. Spectrosc. Radiative Transfer, 111, 1130
Wang L., Kassi S., Liu A. W., Hu S. M., Campargue A., 2011, J. Quant. Spectrosc. Radiative Transfer, 112, 937
Waterman P. C., 1971, Phys. Rev. D., 3, 825
Weck P. F., Stancil P. C., Kirby K., 2003a, J. Chem. Phys., 118, 9997
Weck P. F., Schweitzer A., Stancil P. C., Hauschildt P. H., Kirby K., 2003b, ApJ, 582, 1059
Wenger C., Champion J. P., 1998, J. Quant. Spectrosc. Radiative Transfer, 59, 471
Wenger C., Champion J. P., Boudon V., 2008, J. Quant. Spectrosc. Radiative Transfer, 109, 2697
Wishart A. W., 1979, MNRAS, 187, 59p
Yamamura I., Tsuji T., Tanabe T., 2010, ApJ, 722, 682
Young A. T., 1981, Applied Opt., 20, 533
Yurchenko S. N., Barber R. J., Yachmenev A., Thiel W., Jensen P., Tennyson J., 2009, J. Phys. Chem., 113, 11845
Yurchenko S. N., Barber R. J., Tennyson J., 2011, MNRAS, 413, 1828
Zugger M., Kasting J. F., Williams D. M., Kane T. J., Philbrick C. R., 2010, ApJ, 723, 1168

This paper has been typeset from a TEX/LATEX file prepared by the author.